

Hadron Showers in a Low-Density Fine-Grained Flash Chamber Calorimeter*

W.J. Womersley, J.K. Walker
The University of Florida, Gainesville, FL 32611

D. Bogert, L. Stutte
Fermi National Accelerator Laboratory, Batavia, IL 60510

J. Bofill^a, J.I. Friedman, S. Fuess, M.C. Goodman^b, H.W. Kendall,
V. Kistiakowsky, T. Lyons, L.S. Osborne, R.E. Pitt^c, B. Strongin, F.E. Taylor
Massachusetts Institute of Technology, Cambridge, MA 02139

M. Abolins, R. Brock, W.G. Cobau, R.W. Hatcher, D. Owen, G.J. Perkins
M. Tartaglia, H. Weerts
Michigan State University, East Lansing, MI 48824

August 25, 1987

^aPresent address: Fermi National Accelerator Laboratory, Batavia, IL 60510

^bPresent address: Argonne National Laboratory, Argonne, IL 60439

^cPresent address: AT&T Bell Laboratories, Naperville, IL 60566

*Submitted to Nucl. Instrum. Methods A



Hadron Showers in a Low-Density Fine-Grained Flash Chamber Calorimeter*

W.J. Womersley, J.K. Walker

University of Florida, Gainesville FL 32611

D. Bogert, L. Stutte

Fermi National Accelerator Laboratory, Batavia IL 60510

J. Bofil^a, J.I. Friedman, S. Fuess, M.C. Goodman^b, H.W. Kendall, V. Kistiakowsky,
T. Lyons, L.S. Osborne, R.E. Pitt^c, B. Strongin, F.E. Taylor
Massachusetts Institute of Technology, Cambridge MA 02139

M. Abolins, R. Brock, W.G. Cobau, R.W. Hatcher, D. Owen, G.J. Perkins,
M. Tartaglia, H. Weerts
Michigan State University, East Lansing MI 48824

August 25, 1987

Abstract

Hadronic showers at six incident particle energies from 33.8 to 415.4 GeV have been studied using the low-density fine-grained flash chamber calorimeter of the Lab C neutrino detector at Fermilab. Transverse distributions of unprecedented fine granularity have been obtained for a range of depths in the shower. Longitudinal energy distributions have been compared with those from iron-scintillator detectors. Some differences are observed which may be attributable to the different relative sensitivity of the two detector types to electromagnetic and hadronic shower components. Both longitudinal and transverse distributions have been parametrized. Fluctuations in energy deposition have been studied. The relative size of the fluctuations is largest near the starting vertex and in the tail of the shower, and falls slowly with increasing beam energy. Correlations between energy deposition in neighboring parts of the shower are observed, and anti-correlation is seen between energy deposition in the peak and in the tail of the shower. Containment lengths and widths have also been measured and parametrized.

^a Present address: Fermi National Accelerator Laboratory, Batavia IL 60510

^b Present address: Argonne National Laboratory, Argonne IL 60439

^c Present address: AT&T Bell Laboratories, Naperville IL 60566

* *Submitted to Nuclear Instruments and Methods in Physics Research A.*

1. Introduction

With colliding beam machines dominating high energy physics, and with center of mass energies continually increasing, growing emphasis has been placed on calorimetry rather than magnetic field bending for the determination of particle momenta and energies. This emphasis is likely to continue at future machines where the multiplicity of final state particles may be so great that individual tracks cannot be resolved, and the observable entity becomes the hadron jet.

Despite this significance, an understanding of the way in which hadrons shower and lose energy in matter is limited by the large number of complicated processes involved^[1]. No fully successful Monte Carlo simulation is available, in contrast to the situation for electromagnetic showers^[2]. Hitherto, experimental data on hadronic showers^[3,4,5,6] have been taken at low energies, usually below 150 GeV, and have concentrated on the longitudinal rather than transverse development of the shower. This is because of the limited transverse segmentation available with "classical" iron-scintillator or lead-scintillator sandwich detectors.

It is the intention of this paper to provide useful results on hadron-induced showers in a sampling calorimeter which add significantly to those previously available. Hadronic shower data were taken over the largest range of energies currently available, with hadrons incident at energies from 33.8 to 415.4 GeV on the Lab C neutrino detector at Fermilab. The calorimetry in this detector is provided by flash chambers interspersed with target material and proportional tubes. The flash chambers offer an unrivaled granularity of ~ 6 mm perpendicular to the shower axis, enabling transverse profiles of high quality to be obtained.

2. Apparatus

2.1 The Test Beam

Data were taken using the NH test beam at the Fermilab neutrino area during the 1985 Tevatron fixed-target run. This beam is intended to provide monoenergetic hadrons for energy and angle calibration of the neutrino detector. A schematic diagram of the beam line is shown in Figure 1. Charged particle triggers were taken simultaneously with the neutrino data-taking for experiment 733 (during the slow spill between the fast neutrino extractions). The results in this paper used positive hadrons at the following six beam energies: 33.8, 52.5, 104.1, 209.2, 315.8, and 415.4 GeV. The energy of the incident hadrons was controlled by their passage through two sets of dipole bending magnets. The

upstream bending set used collimators to restrict the aperture available to particles, and in the downstream set four trigger counters defined the beam trajectory into the Lab C detector. The beam entered the calorimeter in the horizontal plane at an angle of 69 mrad to the detector axis. The particle composition at each beam setting was determined using a threshold gas Čerenkov counter in the beamline just upstream of the detector. The momentum bite was calculated from the beamline optics to be $\Delta p/p \sim 3\%$ ^[7] and was checked with the Čerenkov data. The calculated composition of the beam at each energy is listed in Appendix A.

2.2 The Calorimeter

The Lab C detector was designed and built to study weak neutral current events in the Fermilab narrow-band neutrino beam (Experiment 594). More recently it has been extensively employed in a quad-triplet neutrino beam at the Tevatron (Experiment 733). An overview of the detector is shown in Figure 2. Here we shall be concerned only with the calorimeter part of the detector. This has been extensively described elsewhere^[8,9,10] and only a brief review will be given here. The calorimeter consists 38 modules, which contain alternating layers of sand or steel-shot target material, interleaved with flash chambers. A single module has 16 layers of flash chambers and target material, with a proportional tube plane between pairs of modules. In total there are 592 flash chambers and 37 proportional planes.

The flash chambers are constructed^[8] from extruded polypropylene panels covering an area $\sim 4\text{ m} \times 4\text{ m}$. Each chamber measured one of three projections in the plane normal to the neutrino beam axis: $+10^\circ$, 90° , and -10° from horizontal. Each panel contains about 600 parallel cells each approximately $5\text{ mm} \times 6\text{ mm}$ in cross-section. High voltage is applied across the panel causing a glow discharge to occur in a 90% neon, 10% helium, $\sim 0.1\%$ argon gas mixture in those cells which are traversed by ionizing particles. The flash chamber readout is accomplished by using magnetostrictive wires to detect the current pulse induced by the plasma discharge in a struck cell. The current pulse is induced in 3 mm wide copper strips roughly 508 mm long glued to the outside surface near the end of each polypropylene cell. The plasma discharge, after propagating down the cell, causes the capacitance between the copper strip and the high voltage electrode to change. This induces a current pulse of roughly 0.5 A to flow through the copper strips to ground. A magnetostrictive wire is laid over a sense wire region connected to each strip. The current pulse from a struck cell launches an acoustic pulse down the magnetostrictive wire. The time of arrival of this pulse at the end of the wire then gives the position of the struck cell.

The flash chamber determination of the hadronic shower energy is measured by counting the total number of hit flash chamber cells. Certain enhancement algorithms are employed to compensate for the saturation which results from the discrete on/off response of the chambers.

The proportional chambers are built from extruded aluminum cells each of which is 2.5 cm×2.5 cm×3.4 m in size. Each cell contains one 50 μm diameter gold-plated tungsten wire. Groups of four neighboring cells are ganged together for readout giving an effective 10 cm transverse segmentation. Alternate chambers have their wires horizontal and vertical. The chambers are filled with a mixture of 90% argon and 10% methane. Planes of proportional tubes are separated by 46 cm, which is roughly half an interaction length. Readout is by 12-bit ADC with no on-line pedestal subtraction.

The calorimeter also contained liquid scintillator planes (separated longitudinally by 2.5 interaction lengths) which were used for a cosmic muon trigger to monitor the operation of the detector.

The transverse segmentation and longitudinal separation of the planes of flash chambers and proportional tubes are summarised in Table 1. The average density of the calorimeter is 1.35 g cm⁻³. This should be contrasted with ~7 g cm⁻³ for an iron-scintillator detector.

Table 1
Detector parameters

Detector	Transverse segmentation	Longitudinal spacing
Flash chamber plane	6 mm	3.2 cm = 4.3 g cm ⁻²
Proportional tube plane	10 cm	46 cm = 62 g cm ⁻²

3. Data Analysis

3.1 Coordinate System

The coordinate system used throughout this paper is based on the hadron shower direction. The axis of the shower, defined to be the track of the incident particle, forms the z axis with $z = 0$ at the shower vertex. It is assumed that the average shower exhibits

Table 2
Numbers of events after cuts for each beam energy

Beam Energy	Number of Events
33.8 GeV	402
52.5 GeV	214
104.1 GeV	222
209.2 GeV	175
315.8 GeV	156
415.4 GeV	511

axial symmetry about this line and so the transverse shape of the shower is defined by one transverse coordinate, here referred to as x^* . Distances in z have been corrected for the inhomogeneities introduced into the calorimeter by the periodic insertion of proportional tube and liquid scintillator planes, and therefore represent the equivalent lengths in uniform material of the same interaction length as the flash chambers and target material.

3.2 Data Selection

Events were selected which met the following criteria:

- a reconstructed vertex within the calorimeter;
- the downstream end of the shower contained within the calorimeter;
- a reconstructed hadron track upstream of the vertex, with slope and intercept within 5σ of the mean.

The numbers of events surviving these cuts are shown in Table 2. Flash chamber hits were processed by removal of "hot-spots" (*i.e.* continually firing cells). These account for no more than a few percent of the total number of cells firing in an event and tend to be well separated from the hadron shower. Proportional tube pulse heights were corrected for variations in pedestal and gas gain^[7].

A typical hadron shower event seen in the flash chambers is shown in Figure 3.

* It should be noted that z is not a radius. Rather, the design of the detector elements to form parallel straight lines means that distributions in z are effectively obtained by integrating over the coordinate perpendicular to the zz plane.

3.3 Correction for Saturation

In order to fully exploit the fine granularity of the flash chambers, it is necessary to compensate for the saturation that occurs as a consequence of the flash chambers discrete on/off response. A method involving binning the flash chamber cells into sets of ten and enhancing the weight of the hits according to the occupancy has been developed for use in neutrino events^[9], but though this gives a reasonable determination of the total hadronic energy and shower angle, for the purposes of this analysis it does not exploit all of the available information: much of the fine granularity of the flash chambers is lost by binning into sets of ten cells. In preference to the ten-cell binning technique, this analysis has concentrated on using information from the proportional tubes in the calorimeter to correct, on average, for the flash chamber saturation. The response of the proportional tubes is linear, as shown in Figure 4.

To determine this saturation correction the high statistics of the neutrino-induced events were therefore used, binned by hadronic shower energy, where the energy scale was determined from the calibration beam. For both proportional tubes and flash chambers, transverse shower profiles were obtained for 20 cm slices in z downstream from the vertex. For proportional tube hits, a corrected pulse height is available giving a good measure of energy deposition, but for flash chambers each cell which fires has equal weight initially. In each case the shower axis was fitted in lieu of an incident hadron track. The sum of proportional tube pulse heights and total number of flash chamber hits were both normalised to the total estimated shower energy to give an estimated energy per unit pulse height and per flash chamber hit. The closest distance between the shower axis and a cell which fired was taken as x , giving a distribution of $d^2E/dx dz$ for each z slice for proportional tubes and for flash chambers. Comparing these two $d^2E/dx dz$ curves obtained for flash chambers and proportional tubes, a purely empirical average enhancement factor, depending on z , x , and the total number of flash chamber cells firing, was derived. When weighted by this enhancement factor the ratio of flash chamber to proportional tube estimates of $d^2E/dx dz$ was required to be flat in x . This method therefore enhances each flash chamber hit according to its position in an average shower of that energy.

The actual form of the enhancement function is listed in Appendix B. The effect of this enhancement on the shower shape is illustrated in Figure 5 which shows the longitudinal energy deposition dE/dz for 104.1 GeV data before and after enhancement. It will be seen that the correction is roughly a factor of two near the shower maximum, becoming less as the shower grows less dense toward the tail. This enhancement is in reasonable agreement with the results of the ten-cell binning technique.

Though derived from neutrino-induced events, studies indicate that, to the accuracy allowed by the lower statistics, the same enhancement function is appropriate for flash chamber energy enhancement in hadron-induced showers.

The level of systematic error introduced by this enhancement correction can be estimated from how close to unity is the ratio of flash chamber to proportional tube energy distributions after correction. It is estimated from neutrino events that the correction is good to a level of about $\pm 15\%$ for $0 < z < 80$ cm and $\pm 10\%$ for $z > 80$ cm.

4. Calorimeter Parameters

4.1 Interaction Length

The interaction length Λ of the calorimeter was determined from fits of the form $A \exp(-z_v/\Lambda)$ to the vertex position z_v . An additional data selection cut was necessary to remove the distortion in the distribution introduced by the requirement that there be sufficient hadron path length upstream of the vertex to allow the track to be fitted. The value of z_v was corrected for inhomogeneities in the calorimeter. The values obtained from the fit are shown in Figure 6. There is no indication of any energy-dependence and therefore the weighted mean of the six values was taken yielding

$$\Lambda = 85.0 \pm 1.7 \text{ cm.}$$

This compares well with the value of 85 cm estimated from counting the amount of material per centimeter in $z^{[10]}$, and is equal to 115 g cm^{-2} of material.

4.2 Radiation Length

Similar calculations give a value of 14 cm for the radiation length X_0 (19 g cm^{-2} of material). The radiation length was not measured experimentally in this analysis, but has been previously determined^[10] to $\sim 20\%$ from multiple scattering of muons and found to be consistent with the calculated value.

5. Longitudinal Shower Profiles

Here we are concerned with the differential deposition of energy dE/dz as a function of z , the distance along the shower axis. This quantity has been reasonably well measured in a number of previous experiments using metal-scintillator sandwich detectors, and these results fitted to analytic parametrizations^[5,6]. Comparison of the results of this experiment with those parametrizations can potentially illuminate the differences in response between

Table 3Coefficients used in the parametrizations of dE/dz . E is in GeV.

This experiment	UA1 parametrization ^[5]	CDHS parametrization ^[6]
$a = -0.670 + 0.606 \ln E$	$a = 0.6165 + 0.3183 \ln E$	$a = 0.7858 + 0.9839 \log_{10} E$
$b = 0.214$	$b = 0.2198$	$b = 0.2900$
$c = a$	$c = a$	$c = a$
$d = 0.765 - 0.083 \ln E$	$d = 0.9099 - 0.0237 \ln E$	$d = 0.9784$
$w = 0.953$	$w = 0.4634$	$w = 1.0319 - 0.36541 \log_{10} E$

a low-density calorimeter such as that used in this experiment and denser metal-scintillator ones.

Figure 7 shows the values of dE/dz obtained for the various incident hadron energies in this experiment. The curves on the figure show the results of fitting with a parametrization of the usual form for dE/dz :

$$\frac{dE}{dz} = k [ws^{a-1}e^{-bs} + (1-w)t^{c-1}e^{-dt}], \quad (1)$$

where $s = z/X_0$ and $t = z/\Lambda$. The normalisation k is fixed by requiring:

$$\int_0^\infty \frac{dE}{dz} dz = E_{\text{beam}}, \quad (2)$$

which implies:

$$k = E_{\text{beam}} / \left(X_0 w \Gamma(a) / b^a + \Lambda (1-w) \Gamma(c) / d^c \right). \quad (3)$$

The values obtained for the coefficients a , b , c , d and w are listed in Table 3 (first column). The equality between a and c was imposed. These parameters are of course strongly correlated. If an approximate value for k is required, to avoid lengthy calculation, then using

$$k \approx (0.458 - 0.050 \ln E) \text{GeV cm}^{-2}$$

will give results correct to about 10%. The fact that the value of w obtained is close to unity means that the showers can almost be described solely in terms of an electromagnetic component, as would happen in a compensating calorimeter with identical hadronic and electromagnetic responses. A similar conclusion could be drawn if w were close to zero.

5.1 Comparison with the Results of Iron-Scintillator Detectors

The values of dE/dz from this experiment have been compared with those from iron-scintillator detectors by comparing with the values predicted by parametrizations due to R.K. Bock *et al.* [5] used by the UA1 experiment, and due to the CDHS experiment [6]. The functional form of these parametrizations is identical to that of equation (1). The coefficients obtained in each case differ. They are listed in Table 3 (second and third columns).

The curves in Figure 8 show the results using these values of all the coefficients. Figure 9 shows what is obtained for the same values of a , b , c and d if w , the relative weight of electromagnetic and hadronic shower components, is simply rescaled to take account of the different sensitivity to electromagnetic and hadronic shower energy of the calorimeter in this experiment compared to an iron-scintillator detector. In fact the critical energy and other parameters should be included too, and the scaling is probably quite complicated. As a first approximation, the rescaled value w_R is obtained by assuming that:

$$\frac{\text{Sensitivity to EM component}}{\text{Sensitivity to hadronic component}} \propto \frac{\Lambda}{X_0}, \quad (4)$$

which leads to:

$$\frac{w_R}{(1 - w_R)} = \frac{(\Lambda/X_0)_{\text{this expt.}}}{(\Lambda/X_0)_{\text{Fe}}} \frac{w}{(1 - w)} \approx 1.57 \frac{w}{(1 - w)}. \quad (5)$$

The uncertainty introduced into the predictions of the parametrization by varying Λ by its measured error is shown by the bands around each of the curves. The errors on the data points are statistical and systematic added in quadrature.

Comparing the various predictions with the results of this experiment, it will be seen that for energies below 200 GeV the data points lie significantly below both the parametrized curves. However the agreement is improved by using the rescaled w_R in place of the original w , though the changes introduced in the predicted curves are not enough to bring them into full agreement with the data. Above 200 GeV the data points fall between the two predictions and the rescaling produces better agreement with the CDHS curve and worse with the UA1 curve.

It would therefore appear that at high energies the data from this experiment are broadly consistent with these parametrizations and lie between the two predictions. Below 200 GeV this experiment indicates lower energy deposition in the tail of the shower than predicted by the UA1 and CDHS parametrizations. This tendency is consistent with what is expected allowing for the different sensitivities to electromagnetic and hadronic

shower components of this calorimeter compared with metal-scintillator detectors. A naïve rescaling of the relative weights of the two components improves the agreement but does not remove all of the discrepancy.

The discrepancy in the tail could perhaps originate from an over-enhancement for flash chamber saturation in the peak of the shower. This explanation is unlikely to be correct, however, because the enhanced flash chamber energies below 200 GeV are in excellent agreement with the proportional tube information. The latter is reliably linear in this energy range.

It must be remembered that the energy response of the scintillators and the critical energy of the iron absorber used in these other experiments will in any case be different from those of the gas counters and absorber material of the Lab C detector. These differences will become more significant at low energies in the tail of the showers.

6. Transverse Shower Profiles

Transverse profiles are obtained assuming axial symmetry of the shower and taking the closest distance between the shower axis and each flash chamber cell as x . The relative and absolute normalisation on all these curves is derived from the requirement that the energy in the whole shower be equal to the beam energy. The quantity plotted is energy deposition $d^2E/dx dz$ as a function of x at constant z (z in bins of 20 cm corresponding to increments of 27 g cm^{-2} in material traversed, or 0.24 interaction lengths). The profiles obtained are shown in Figures 10(a)-(f). The errors on the data points are statistical only; systematic errors from the enhancement technique are estimated to be $\pm 15\%$ for $0 < z < 80 \text{ cm}$ and $\pm 10\%$ for $z > 80 \text{ cm}$.

The transverse profiles are strongly peaked toward $x = 0$, with no indication of a plateau in energy deposition toward the center of the shower. As z increases the width of the transverse profile grows.

The curves drawn on the transverse profiles are exponentials of the form:

$$dE/dx = ke^{-x/g}. \quad (6)$$

where g has been fitted to the data to yield:

$$\begin{aligned} g(z) &= g_1 + g_2 z \\ &= (-4.24 + 1.93 \ln E) + (0.184 - 0.026 \ln E)z, \end{aligned} \quad (7)$$

where E is in GeV, and z in centimeters. To use these transverse distributions for other materials, it may be more useful to convert x to an amount of material per square centimeter. The average density of the calorimeter is independent of angle, so $1 \text{ cm} = 1.35 \text{ g cm}^{-2}$ in the transverse direction.

These exponentials are the simplest transverse distribution which gives reasonable agreement with the data. They do not describe the very early part of the shower very well but are close to the data points in the peak and broad tail of the shower where shower widths are more likely to be important considerations. More complicated functions were tried but did not give a worthwhile improvement in the quality of the transverse fit.

7. Overall Parametrization

The parametrizations of the longitudinal and transverse energy deposition may be combined to yield an overall parametrization for hadron showers in this experiment:

$$\frac{d^2 E}{dx dz} = k [w s^{(a-1)} e^{-bs} + (1-w)t^{(c-1)} e^{-dt}] [e^{-x/(g_1+g_2z)}], \quad (8)$$

where $a = c = -0.670 + 0.606 \ln E$, $b = 0.214$, $d = 0.765 - 0.083 \ln E$, $w = 0.953$, $g_1 = -4.24 + 1.93 \ln E$, $g_2 = (0.184 - 0.026 \ln E) \text{ cm}^{-1}$, $s = z/X_0 = z/14 \text{ cm}$, $t = z/\Lambda = z/85 \text{ cm}$, x is measured in cm and E is measured in GeV, and k is fixed by the requirement that the total energy in the shower be equal to the energy of the incident particle. An approximate value of k , good to about 10%, is given by:

$$k \approx (0.458 - 0.050 \ln E) / (g_1 + g_2 z) \text{ GeV cm}^{-2}.$$

8. Visualisation of Shower Shapes

One may plot the measured values of $d^2 E/dx dz$ on the xz plane to obtain a visualisation of the energy deposition in the average shower at each energy. The information from all three flash chamber views is combined in the transverse profiles which gives higher statistics but means that left-right symmetry is assumed. In the visualisation one therefore necessarily obtains the same value of energy deposition for positive and negative x . Such representations are shown in Figure 11(a)-(f). The single "thermometer" cell shows a deposition of 0.1 GeV cm^{-2} in each plot.

9. Fluctuations

It is well-known that hadronic showers are subject to large fluctuations in energy deposition. It is therefore worthwhile to investigate such effects, though since the enhancement for flash chamber hits is based on an average shower shape it is not strictly valid for a study of fluctuations. The fluctuations will be systematically underestimated by this technique.

Figures 12(a)-(f) show the magnitude of the variation in dE/dz as a function of z . The two curves are the mean energy deposition, and the mean plus root-mean-square about the mean. Figure 13 shows the root-mean-square as a fraction of the mean as a function of z . It will be seen that in all cases the fluctuations are large, with an r.m.s. always greater than the mean. The fractional fluctuations are smallest in the middle part of the shower, and are larger both for very small z , and in the tail of the shower. This is consistent with the fluctuations being greatest in the regions where average multiplicity in the shower is lowest, as one might expect.

It is perhaps interesting that for all incident hadron energies, at the peak of the shower the r.m.s. is close to being equal to the mean. This relationship is what would be expected in the limit of large multiplicity if the energy deposition were simply proportional to the number of particles, with the number of particles distributed according to a Furry distribution^[11]. Such a distribution describes the number of particles in an electromagnetic shower in the limit that production rate is much greater than stopping rate; this condition is probably most nearly reached at the peak of the shower development. It would therefore seem that a similar distribution may describe the number of particles present in these hadronic showers.

One may also investigate the energy-dependence of the size of fluctuations. Averaging over $0 < z < 600$ cm, the values shown in Figure 14 are obtained for r.m.s./mean energy deposition $\sigma/(dE/dz)$ as a function of incident hadron energy E_{beam} . As the energy rises, there is a slow fall in the fractional size of the fluctuations. One possibility is that the fluctuations are dependent on some multiplicity increasing as $\ln E_{\text{beam}}$, leading to:

$$\frac{\sigma}{dE/dz} \propto \frac{1}{\sqrt{\ln E_{\text{beam}}}}, \quad (9)$$

and hence:

$$1/\left(\frac{\sigma}{dE/dz}\right)^2 \propto \ln E_{\text{beam}}. \quad (10)$$

This quantity $1/\left(\frac{\sigma}{dE/dx}\right)^2$ is plotted as a function of $\ln E_{\text{beam}}$ in Figure 15 and shows a reasonable straight-line behavior. This supports the view that the smaller fractional size of the fluctuations at higher energies is due to higher average multiplicity in the shower.

10. Correlations

The fluctuations in a hadronic shower are also expected to be highly correlated. This is borne out by results presented here. The energy deposited in the range $80 < z < 100$ cm, which is usually somewhere toward the center of the shower, has been compared with the energy recorded in the same event for three other ranges of z : $100 < z < 120$ cm, $200 < z < 220$ cm and $300 < z < 320$ cm. The resulting scatter plots are shown in Figure 16(a)-(f). A strong correlation will be seen between the energies in the 80-100 cm and 100-120 cm intervals. This is expected, since the average range of both hadronically and electromagnetically interacting particles in the calorimeter is greater than the 20 cm separating the centers of these two bins, and so an excess of particles and hence energy seen in the first bin will tend to be seen in the second.

The correlation is washed out when comparing the energies in the intervals 80-100 cm and 200-220 cm (120 cm separation). The "correlation length" in the shower would therefore appear to be of the order of one interaction length (85 cm), as expected.

When comparing the energies in the ranges 80-100 cm and 300-320 cm there are indications of anti-correlation. This is only reasonable, since for example a fluctuation to large energy early in the shower means that there is less energy available for deposition later.

11. Containment

Determining the amount of calorimeter material necessary to contain a certain fraction of the energy in an average shower is of great interest for the design of calorimeter systems.

11.1 Energy Leakage

By integrating the results presented earlier for dE/dz , one may obtain the plots shown in Figure 17 of the energy leakage, *i.e.* the fraction of energy deposited downstream of z as a function of z . A similar procedure may be used in the transverse plane to obtain the results of Figure 18 which shows the fractional energy leakage in the transverse coordinate x .

11.2 Containment Lengths

From the plots of energy leakage, the lengths necessary to contain 90, 95 and 99% of the shower energy have been extracted. In Figure 19 these lengths are plotted as a function of incident hadron energy. The lengths have been converted to numbers of interaction lengths and the errors include a 2% contribution in quadrature from the experimental uncertainty on the interaction length. The 415.4 GeV data point appears to be slightly low compared with the general trend. This may be due to loss of particles from the sides of the calorimeter at these high energies. There is no indication of any significant losses through the downstream end of the calorimeter. The containment lengths have been fitted by the following parametrizations (where L is measured in interaction lengths and E in GeV):

$$\begin{aligned}L(90\%) &= -0.371 + 0.813 \ln E, \\L(95\%) &= 0.101 + 0.870 \ln E, \\L(99\%) &= 0.642 + 1.063 \ln E.\end{aligned}\tag{11}$$

These lines are shown on the figure. They may be compared with the parametrizations of the 95% containment length due to Holder *et al.*^[4] and Prokhoroskin^[12]. Both of these parametrizations are based on iron-scintillator data in the range 10–140 GeV. In general the results of this experiment are reasonably consistent with these parametrizations at low energy, but suggest a somewhat steeper rise with $\ln E$.

The results presented here refer to *the length of the shower relative to its starting vertex*, and therefore to determine the total length of calorimeter that is necessary for containment at any given probability one must strictly convolute with the probability distribution $e^{-x/\Lambda}$ of the vertex, though to a first approximation one may add one interaction length to those plotted.

The results are also for the mean containment length and do not indicate anything about the fluctuations about this length. Such fluctuations are likely to be large, as is indicated by the considerable increase in the length required for 99% compared with 95% containment.

11.3 Lateral Containment

Figure 20 shows the half-widths required for 90, 95 and 99% containment as a function of incident hadron energy. It will be seen that there is a very much slower increase in the containment widths with energy compared to the containment lengths. Indeed the 90% containment half-width remains essentially constant from 33.8 to 415.4 GeV, a perhaps

surprising result. The widths have been fitted by the following parametrizations (where E is measured in GeV):

$$\begin{aligned}
 W(90\%) &= (34.5 + 1.22 \ln E) \text{ cm} = (46.6 + 1.65 \ln E) \text{ g cm}^{-2}, \\
 W(95\%) &= (47.2 + 2.58 \ln E) \text{ cm} = (63.7 + 3.48 \ln E) \text{ g cm}^{-2}, \\
 W(99\%) &= (56.6 + 8.71 \ln E) \text{ cm} = (76.4 + 11.7 \ln E) \text{ g cm}^{-2}.
 \end{aligned}
 \tag{12}$$

These lines are shown on the figure. Overall these results are consistent with the “rule of thumb” that a shower is contained within a cylinder of radius equal to the interaction length of the calorimeter material^[13].

12. Conclusions

In conclusion, the flash chamber calorimetry of the Lab C neutrino detector has been used to study the properties of hadronic showers at six incident hadron energies from 33.8 to 415.4 GeV. The effects of the saturation of the flash chambers have been removed using an analytic function based on the response of proportional tubes in an average shower.

Transverse and longitudinal energy deposition have been studied, and parametrizations for each obtained. The detector design has enabled transverse distributions of a granularity never previously seen to be obtained for a range of depths in the shower.

The longitudinal distributions have been compared with parametrizations of iron-scintillator calorimeter results. Lower energy deposition is observed in the tail of the shower at low incident hadron energies compared with these parametrizations. This tendency is however consistent with what would be expected from the different sensitivities of this detector to electromagnetic and hadronic shower components compared with an iron-scintillator detector.

The fluctuations of energy deposition about the mean value have been investigated. The fluctuations are large, with a root-mean-square about the mean which is always larger than the mean. The fractional size of the fluctuations is found to be larger early and late in the shower with a minimum near the shower peak. The fluctuations also become relatively smaller with increasing incident hadron energy. Correlations between energy deposition in neighboring parts of the shower are observed, and anti-correlation is seen between energy deposition in the peak and in the tail of the shower.

Containment lengths and widths have also been studied. The containment length is found to rise logarithmically with incident hadron energy, while the width is much less dependent upon energy.

Acknowledgments

We should like to thank the National Science Foundation and the U.S. Department of Energy for funding this work. The experiment would not have been possible without the fine technical support of Fermilab, MIT, MSU, and UF.

Appendix A — Beam Composition

The table below shows the calculated fractional composition of the hadron beam at each energy. Decays in flight are neglected.

Beam Energy	π (%)	K (%)	p (%)
33.8 GeV	86	9	5
52.5 GeV	83	9	8
104.1 GeV	76	8	17
209.2 GeV	60	6	34
315.8 GeV	39	4	57
415.4 GeV	20	3	77

Appendix B — The Enhancement Function

Let x and z be the uncorrected coordinates in centimeters of a flash chamber hit, using the coordinate system described earlier; and H be the value of $\frac{1}{1000} \times$ (total number of flash chamber cells firing) in the event. Then the enhanced weight of the flash chamber hit is

$$C(x, z, H) = C_0 C_3 / C_1, \quad (13)$$

where:

$$C_0 = 1 / \left\{ 1 - (0.82 - 0.00128z)e^{-z/33.4} \right\};$$

$$C_1 = 1 + (0.75 - 0.252H - 0.0015z + 0.00032zH + C_2)e^{-z/(5+0.0375z)};$$

$$C_2 = \begin{cases} 2.82e^{-z/16.88(H-2.815)}, & \text{if } H > 2.815 \\ 0, & \text{otherwise;} \end{cases}$$

$$C_3 = \begin{cases} (z - 250)/200, & \text{if } z > 450 \\ 1, & \text{otherwise.} \end{cases}$$

References

- [1] R. Wigmans, CERN preprint EF/86-18 (EP/86-141), 1986
- [2] E. Longo and I. Sesteli, Nucl. Inst. & Meth. **128** (1975) 283
- [3] B.C. Barish *et al.* Nucl. Inst. & Meth. **116** (1974) 413
B.C. Barish *et al.* Nucl. Inst. & Meth. **130** (1975) 49
D.L. Cheshire *et al.* Nucl. Inst. & Meth. **126** (1975) 253
B. Friend *et al.* Nucl. Inst. & Meth. **136** (1976) 505
H. Abramowicz *et al.* Nucl. Inst. & Meth. **180** (1981) 429
- [4] M. Holder *et al.* Nucl. Inst. & Meth. **151** (1978) 69
- [5] R.K. Bock, T. Hansl-Kozanecka, and T.P. Shah,
Nucl. Instr. & Meth. **186** (1981) 533
- [6] E. Hughes, CDHS Internal Report, "Measurement of Hadronic and Electromagnetic Shower Development between 10 GeV and 140 GeV by an Iron-Scintillator Calorimeter", August 1986 (unpublished)
- [7] M. Tartaglia, in Proc. of the Gas Sampling Calorimetry Workshop II, Fermilab, 1985, pp 259-290 (Fermi Nat. Accel. Lab., 1985)
- [8] F.E. Taylor *et al.*, IEEE Trans. Nuc. Sci. **NS 27** (1980) 30
- [9] D. Bogert *et al.*, IEEE Trans. Nuc. Sci. **NS 29** (1982) 363
- [10] M. Tartaglia, Ph.D. thesis, Massachusetts Institute of Technology, 1984
- [11] F.W. Furry, Phys. Rev. **52** (1937) 569
- [12] Yu.D. Prokhoskin, in Proc. of 2nd ICFA Workshop on Possibilities and Limitations of Accelerators and Detectors, Les Diablerets, October 1979; edited by U. Amaldi (CERN, June 1980)
- [13] U. Amaldi, in Proc. of Int. Conf. on Experimentation at LEP, Uppsala, June 1980 (CERN report EP/80-212, 1980)

Figure Captions

Figure 1

A schematic diagram showing the NH hadron test beam at the Fermilab neutrino area.

Figure 2

An overview of the Lab C neutrino detector, showing details of the construction.

Figure 3

A typical hadron-induced event in the flash chambers. The three views correspond to the three orientations of the flash chamber cells. Beam energy was 315.8 GeV.

Figure 4

Response of the proportional tubes after pedestal subtraction and gain correction. The quantity plotted is the total proportional tube pulse height in hadron-induced events as a function of incident particle energy.

Figure 5

Longitudinal energy deposition dE/dz as a function of z , plotted for raw (open circles) and corrected (closed circles) flash chamber hits from 104.1 GeV data. The corrected hits are weighted by the enhancement function as described in the text; the raw hits have unit weight.

Figure 6

Fitted values of the incident hadron interaction length as a function of incident hadron energy. The horizontal dashed line shows the value of the weighted mean. Lengths are in centimeters; $1 \text{ cm} = 1.35 \text{ g cm}^{-2}$. Note the suppressed zero on the vertical axis.

Figure 7

Longitudinal energy deposition dE/dz as a function of z , the distance along the shower axis. Errors are statistical and systematic in quadrature. The curves are parametrizations of the data as described in the text. Longitudinal distance is measured in centimeters; $100 \text{ cm} = 1.18 \text{ interaction lengths} = 135 \text{ g cm}^{-2}$.

Figure 8

Longitudinal energy deposition dE/dz compared with the predictions of the parametrizations of references [5] (solid line) and [6] (dashed line). The dotted lines forming a band

around each curve show the effect on the prediction when the interaction length is varied by its measured error.

Figure 9

As Figure 8 but with w , the relative weight of electromagnetic and hadronic contributions to the predicted curves rescaled as described in the text.

Figure 10

Measured energy deposition $d^2E/dx dz$ as a function of x for 20 cm bins of z . Errors are statistical only. The curves are exponentials with a width given by a fit as described in the text. The transverse coordinate is in centimeters; $1 \text{ cm} = 1.35 \text{ g cm}^{-2}$.

Figure 11

Three-dimensional representation of energy deposition in an average hadronic shower. The beam particle enters as shown. Longitudinal scale is 0 to 600 cm and transverse scale is -50 to 50 cm. The vertical scale is shown by the column representing 0.1 Gev/cm^2 .

Figure 12

Fluctuations in longitudinal energy deposition dE/dz as a function of z . The solid line links the measured mean deposition. The dashed line shows the mean value plus the root-mean-square of the variation about the mean.

Figure 13

Fractional size of fluctuations in dE/dz as a function of z . The plotted quantity is the r.m.s. σ of dE/dz about the mean, divided by the mean value $\langle dE/dz \rangle$.

Figure 14

Variation of average fluctuations in longitudinal energy deposition as a function of energy. The quantity plotted for each energy is the average over z of $\sigma/\langle dE/dz \rangle$.

Figure 15

The same data as in Figure 14 but presented as $1/(\sigma/\langle dE/dz \rangle)^2$ to show the approximately logarithmic rise with energy.

Figure 16

Scatter plots showing the relationship for each event between the energy deposited in the interval $80 < z < 100$ cm and that in the intervals $100 < z < 120$ cm, $200 < z < 220$ cm and $300 < z < 320$ cm.

Figure 17

Fractional energy leakage as a function of z .

Figure 18

Fractional energy leakage as a function of x .

Figure 19

Containment lengths as a function of incident hadron energy. The errors include a contribution of 2% from the experimental uncertainty in the interaction length.

The solid lines show the parametrizations of these data given in the text. The dashed line shows the parametrization of reference [4] and the dot-dashed line that of reference [12] for 95% containment, extrapolated from data below 150 GeV, taking $\Lambda = 19$ cm for the iron-scintillator detectors used.

Figure 20

Containment half-widths as a function of incident hadron energy. Errors on the data points are statistical only.

BEAM LINE LAYOUT

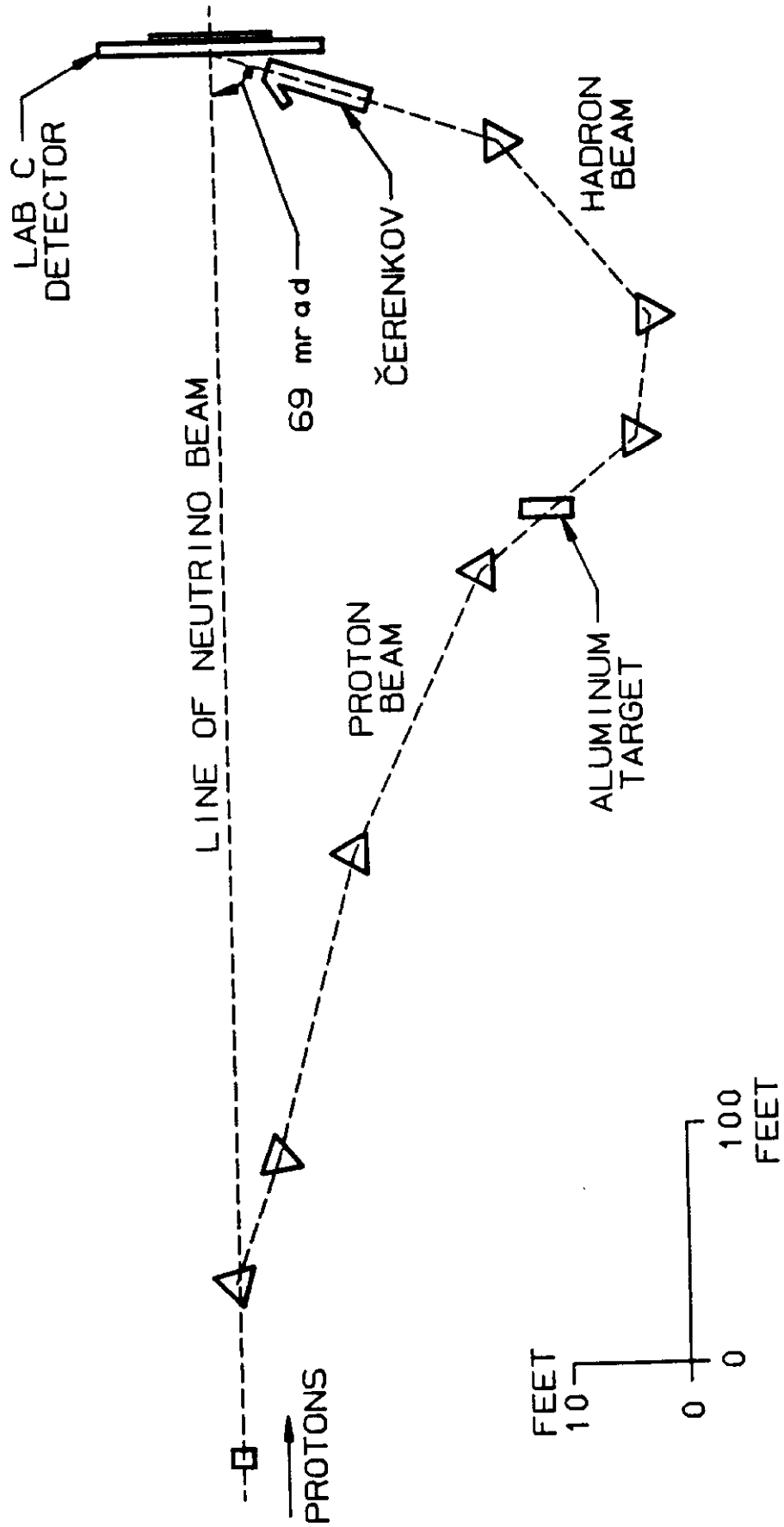


Figure 1

LAB C NEUTRINO DETECTOR

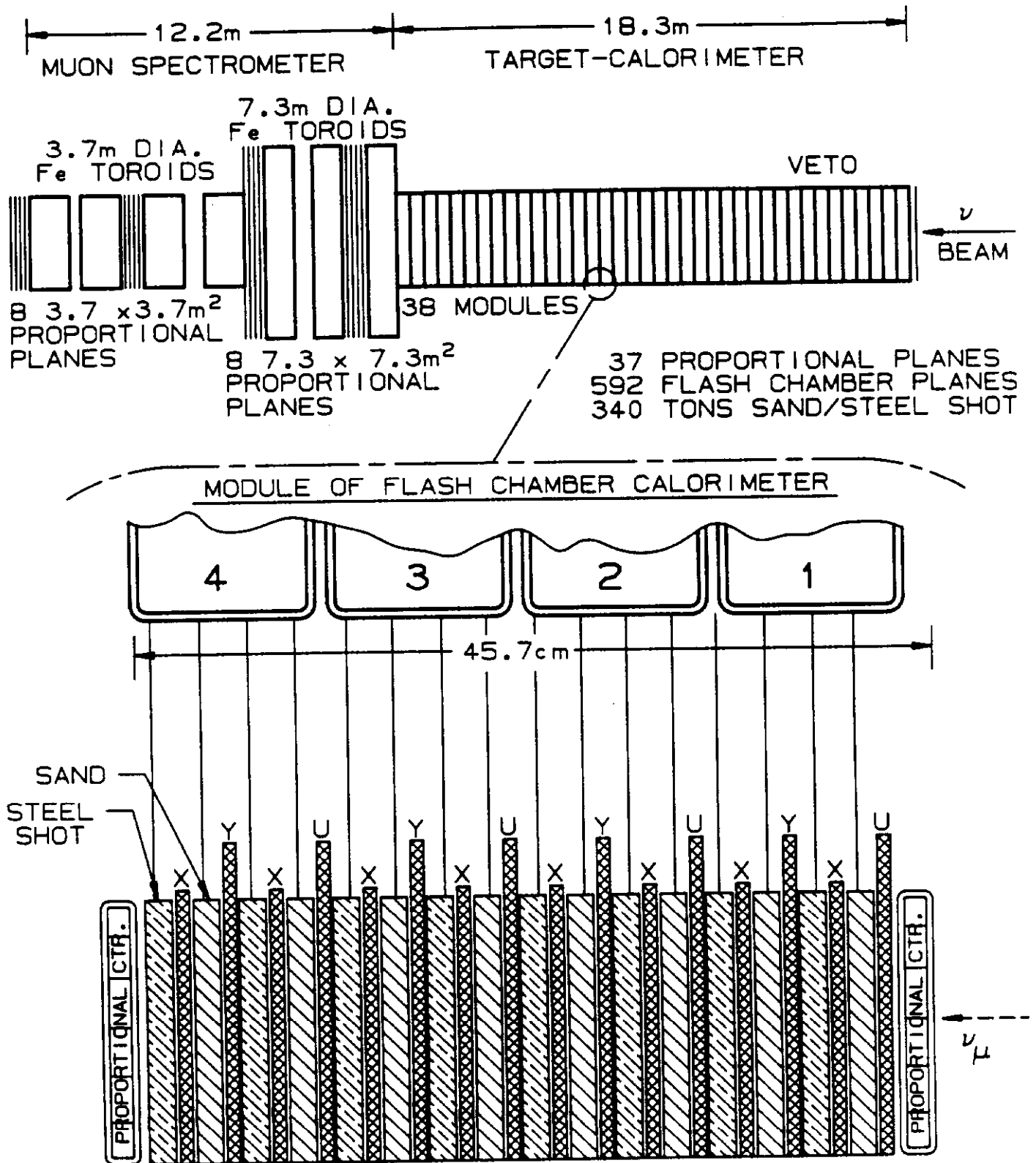


Figure 2

RUN 7106 EVENT 13
FC HITS= 69d7

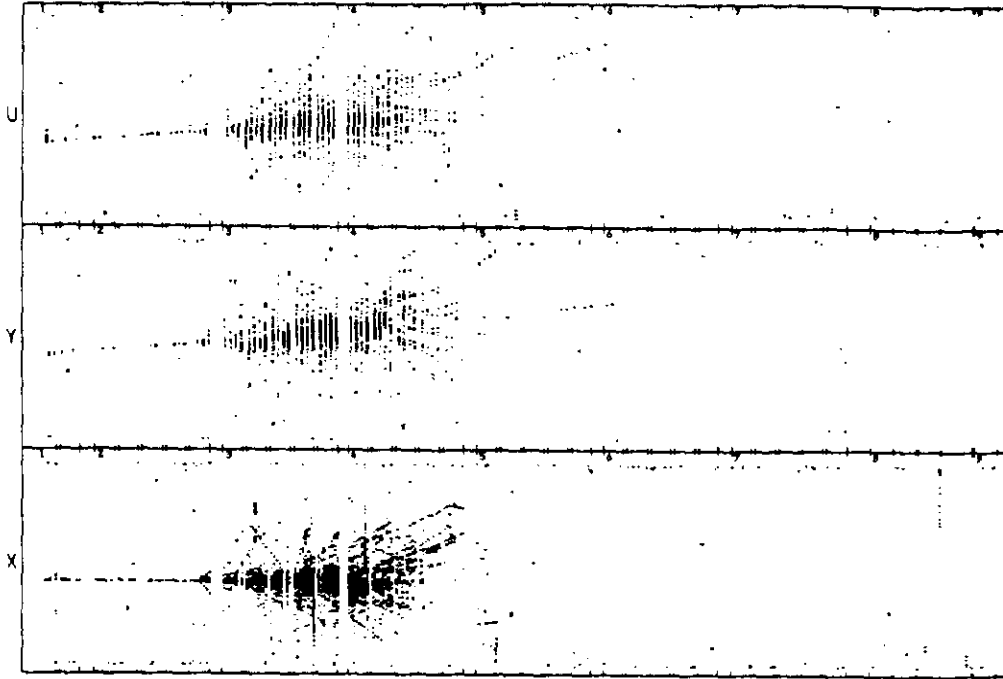


Figure 3

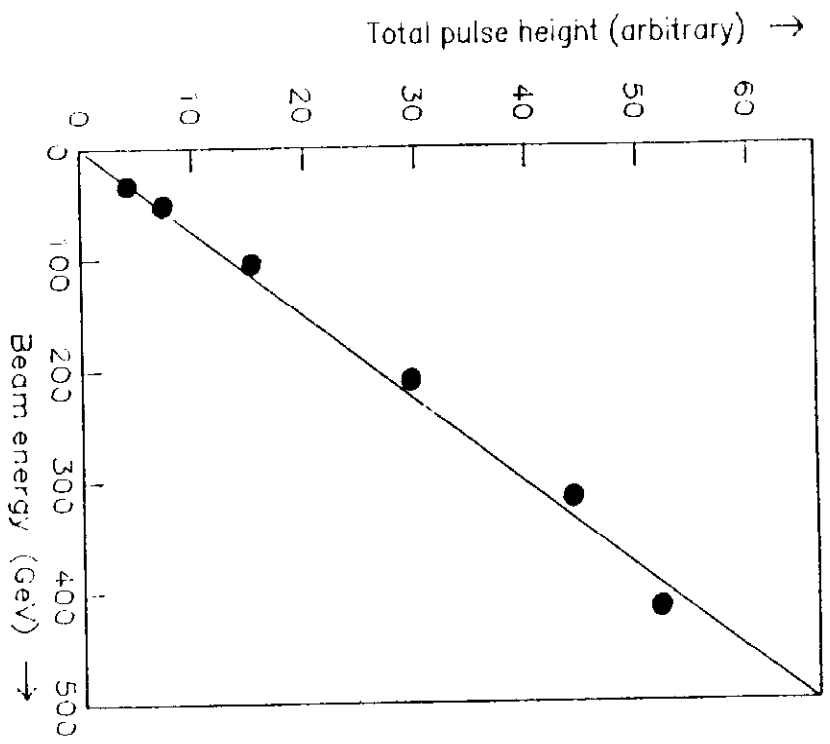


Figure 4

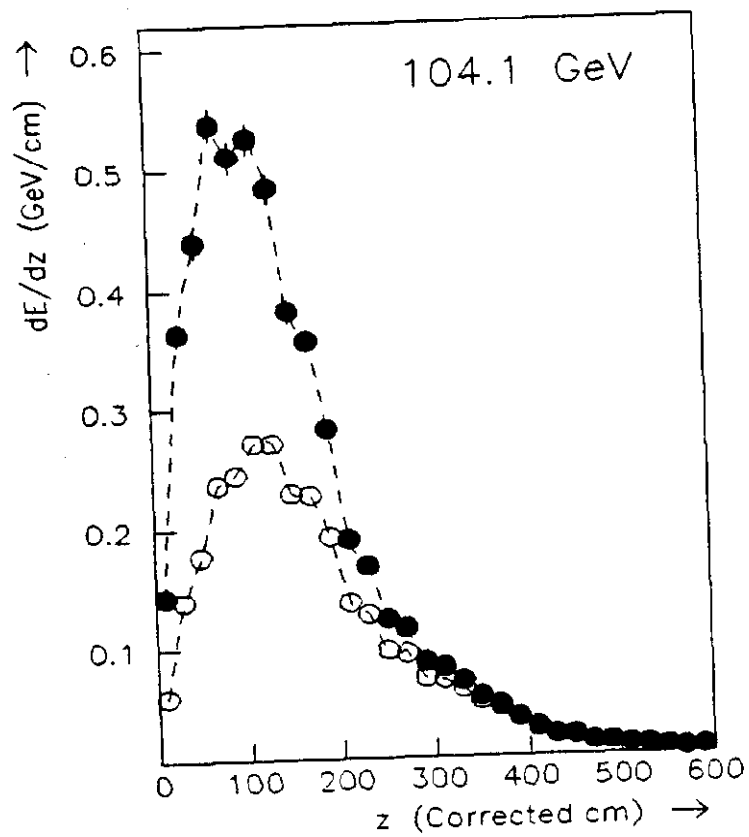


Figure 5

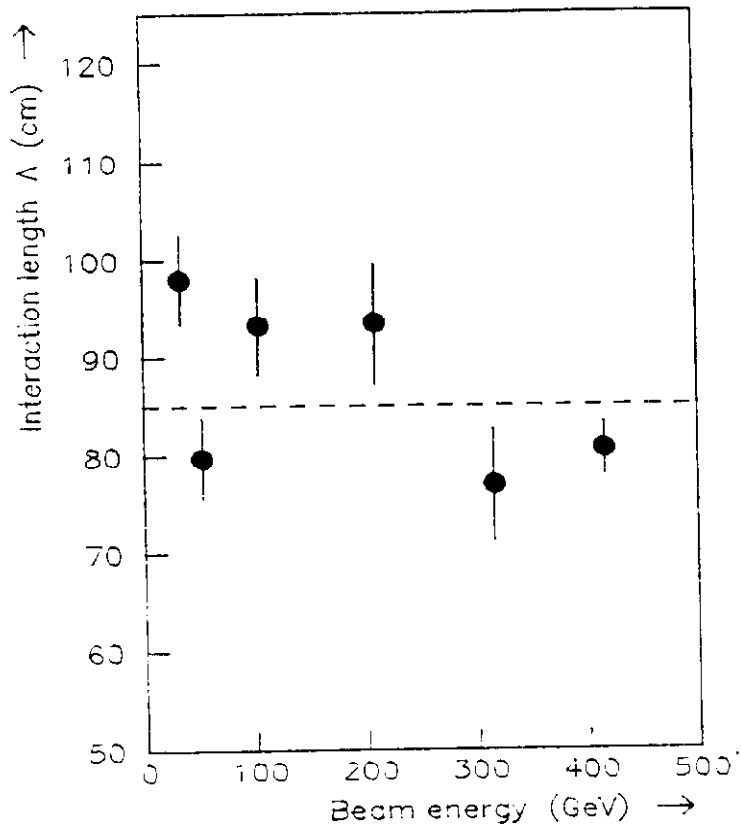


Figure 6

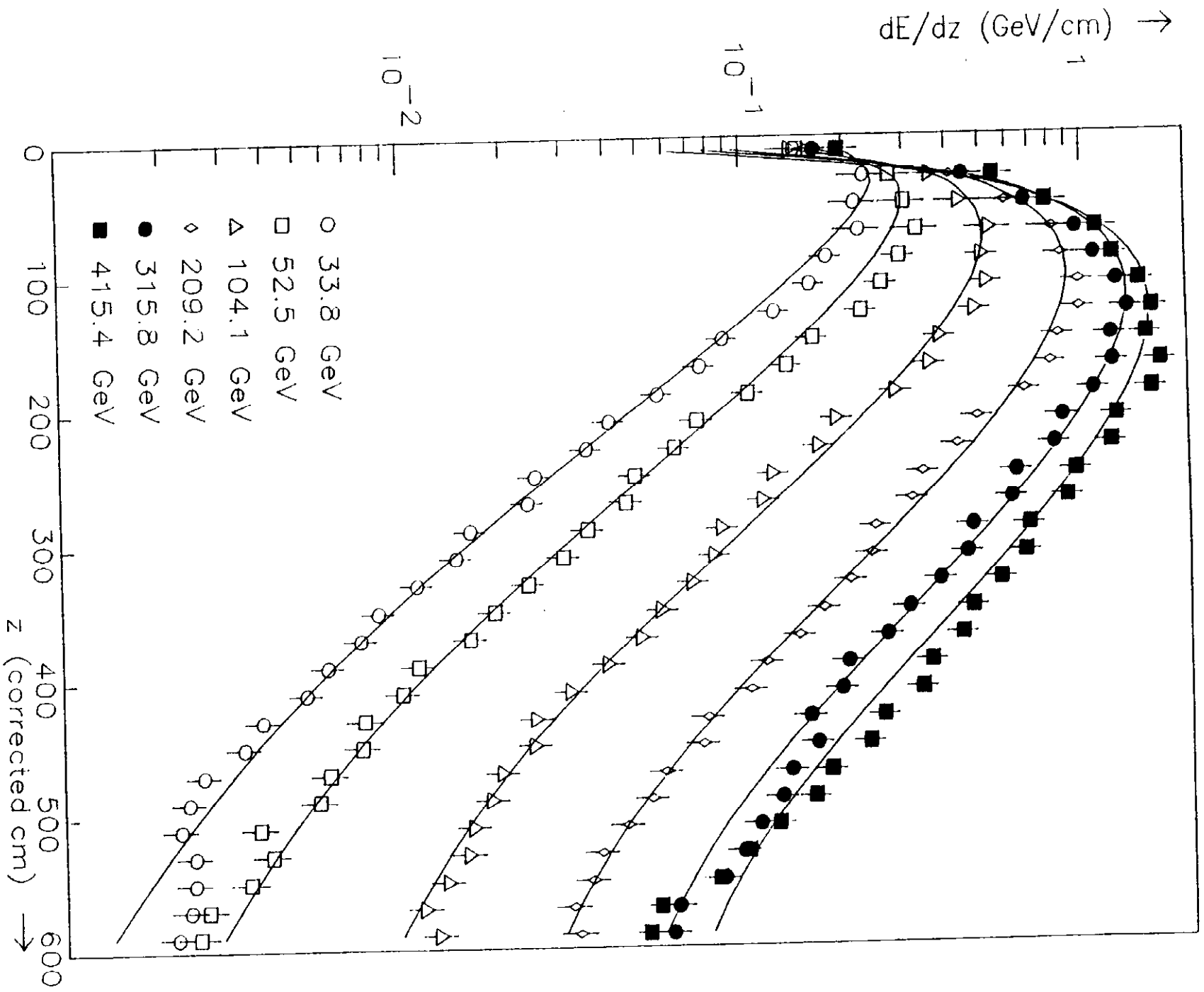


Figure 7

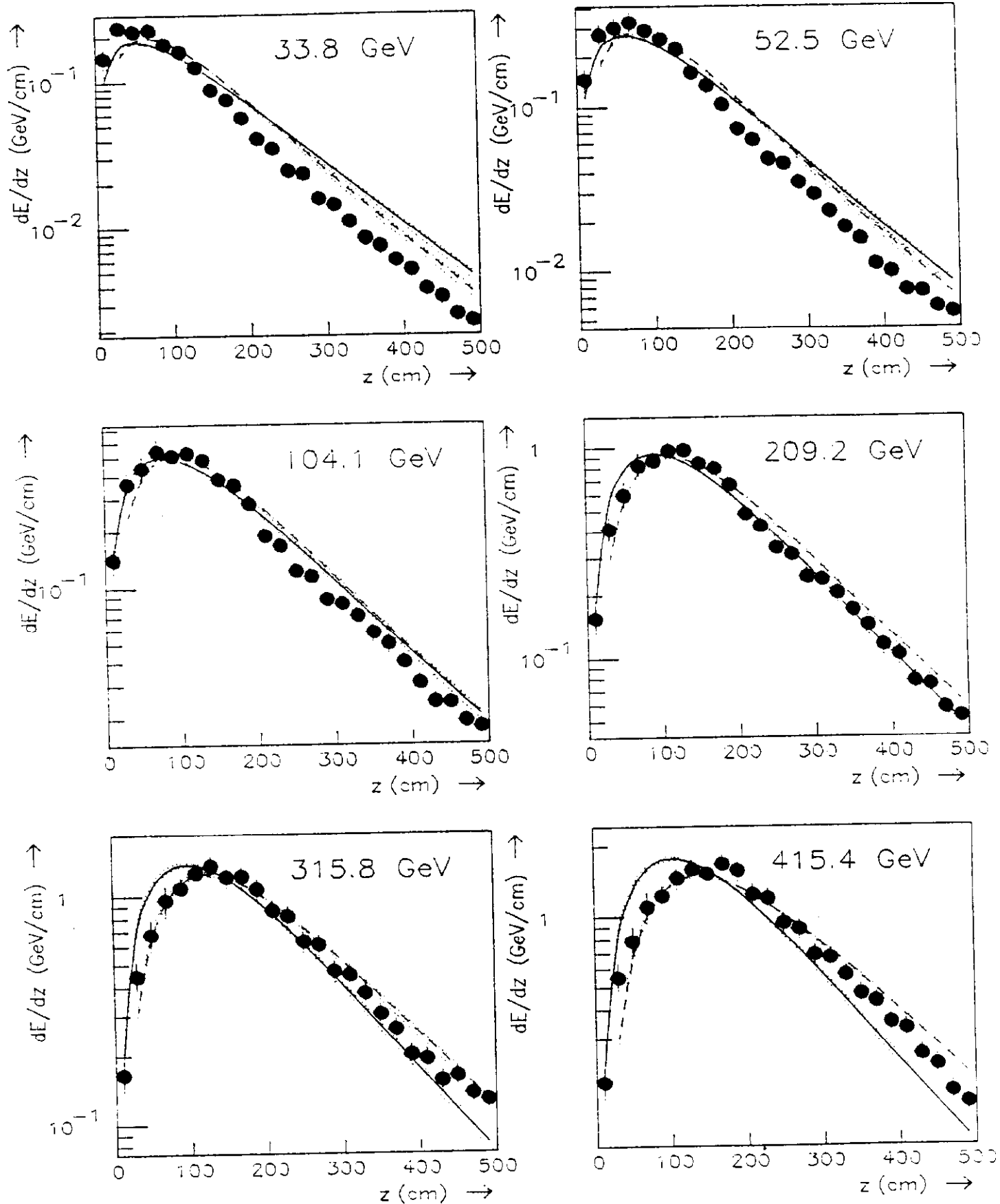


Figure 8

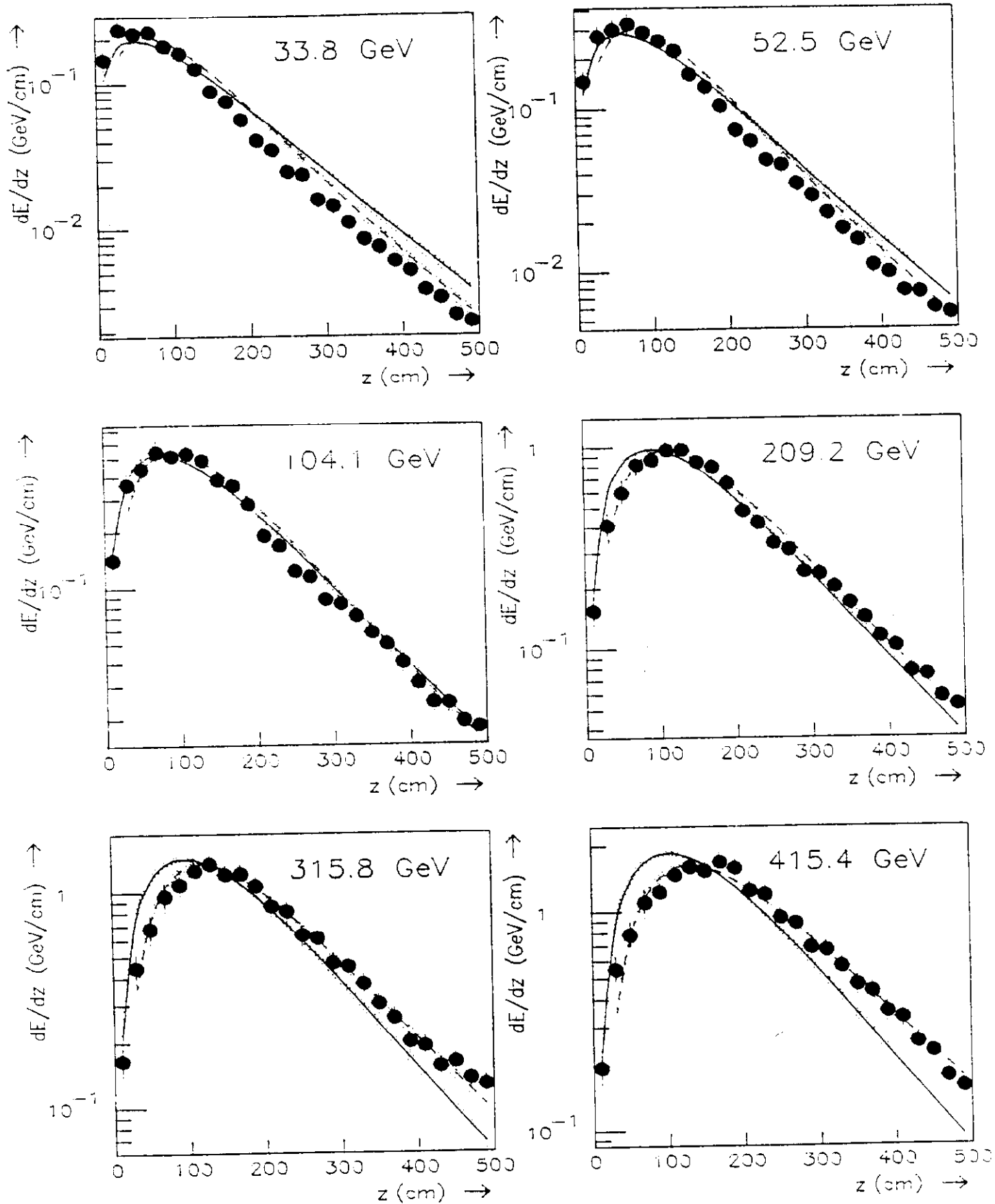


Figure 9

33.8 GeV

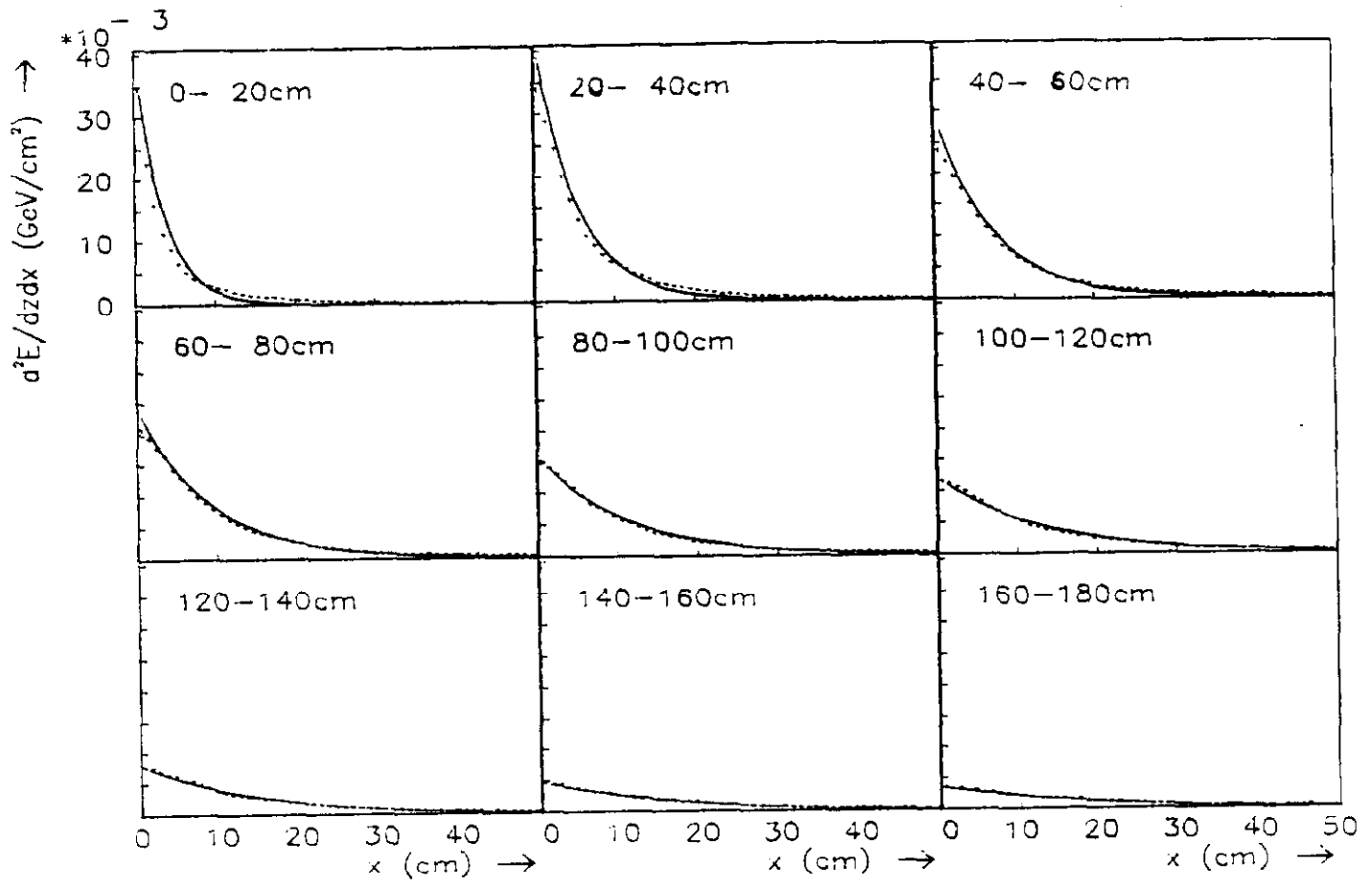


Figure 10(a)

52.5 GeV

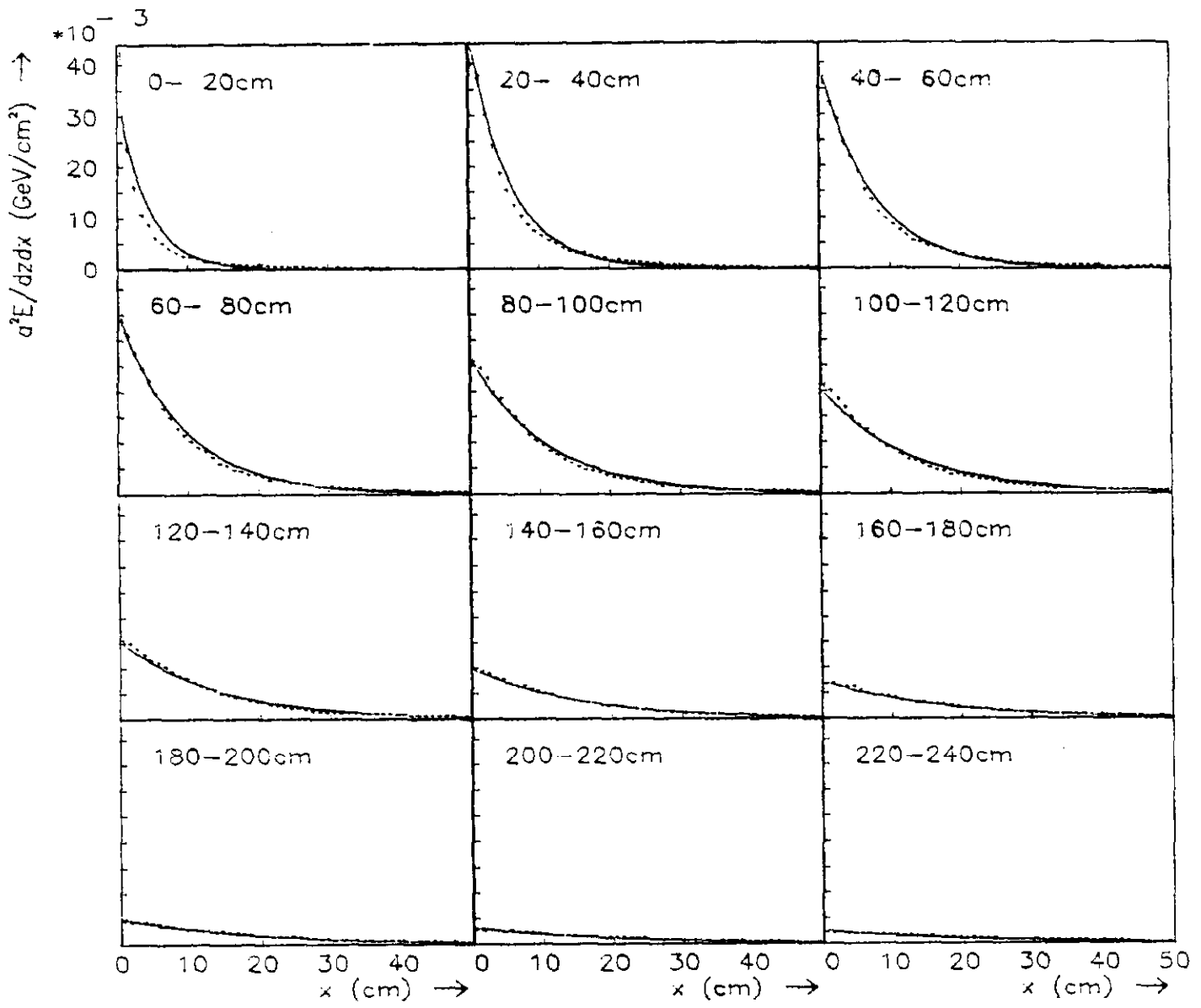


Figure 10(b)

104.1 GeV

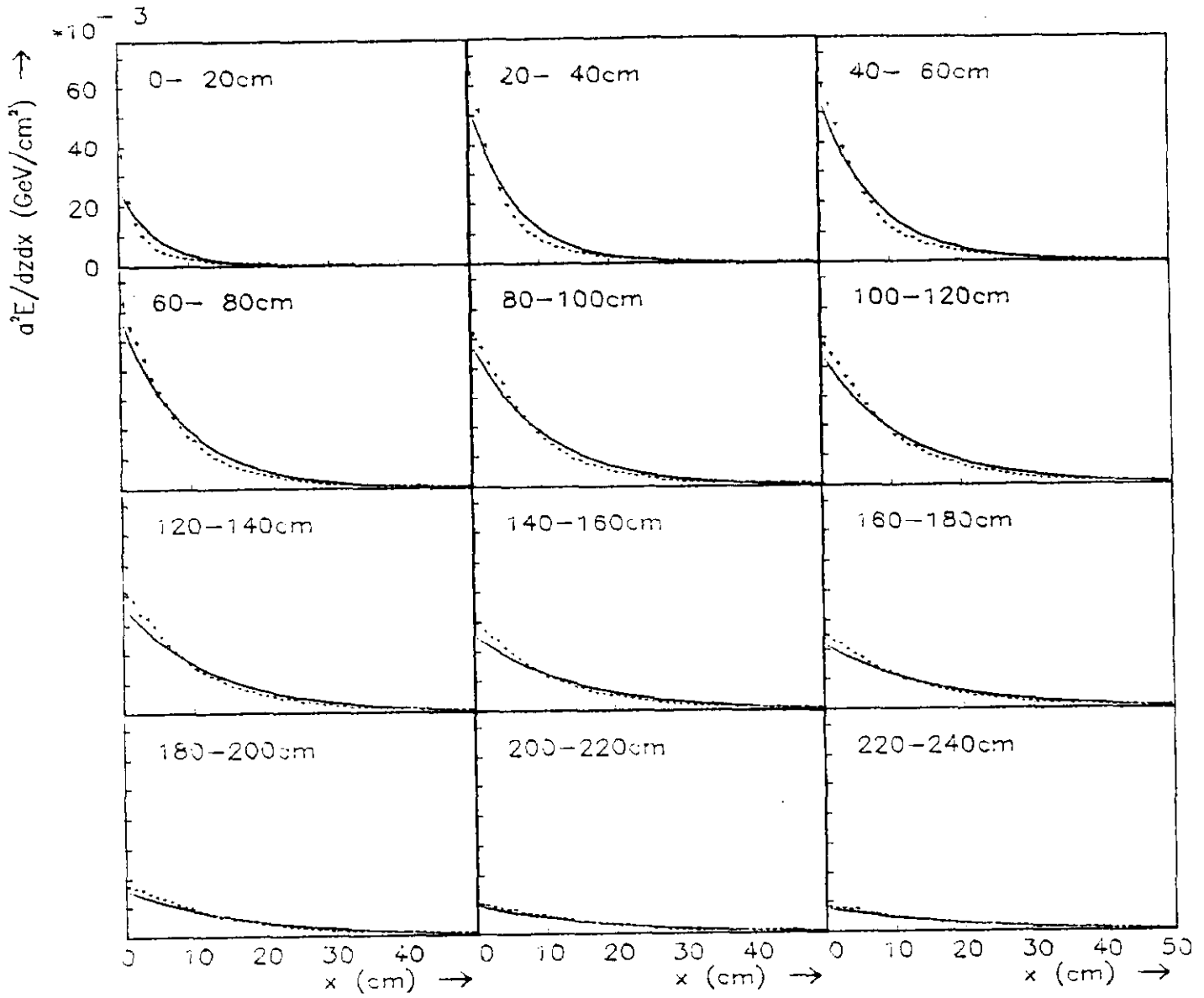


Figure 10(c)

209.2 GeV

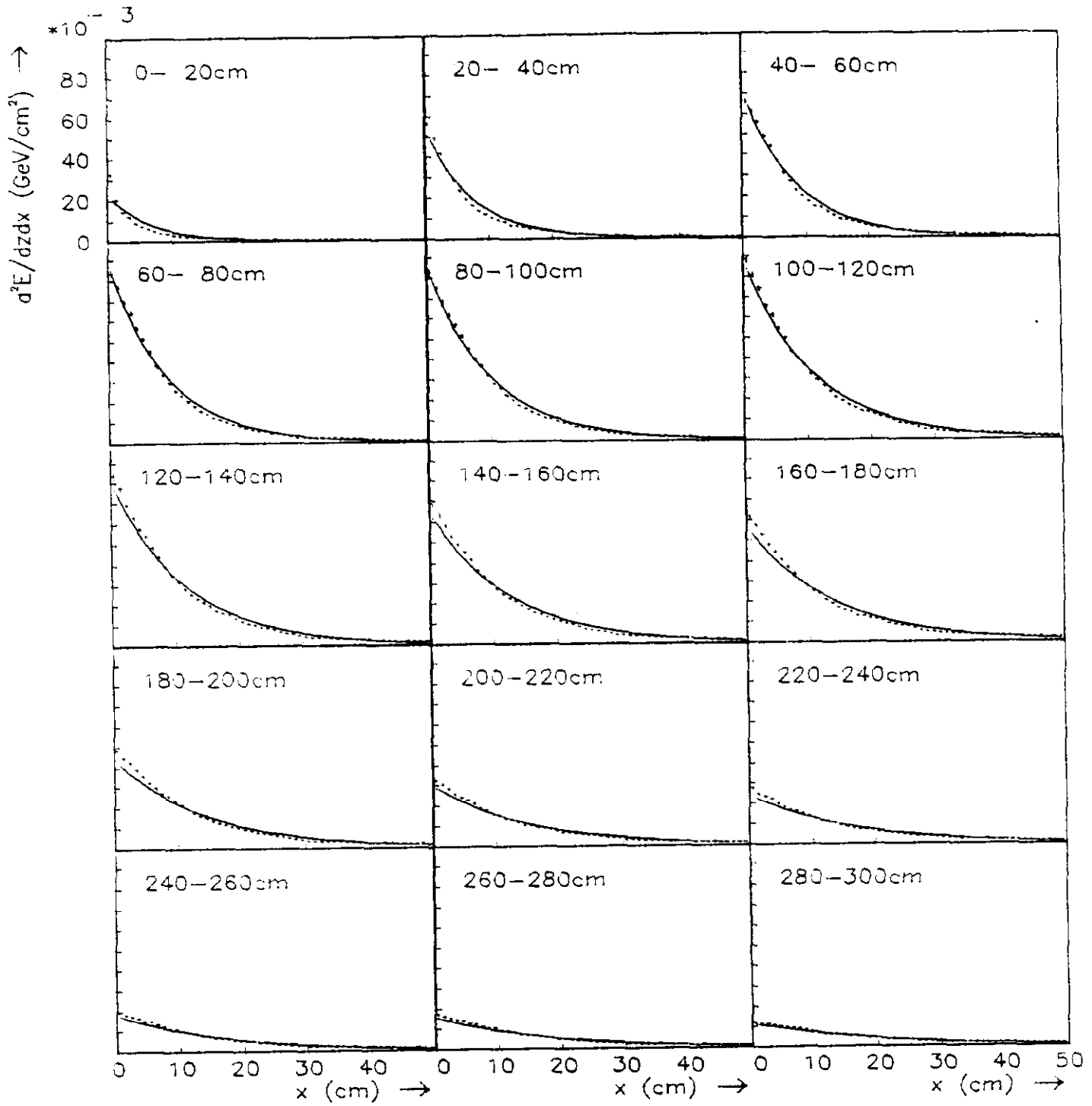


Figure 10(d)

315.8 GeV

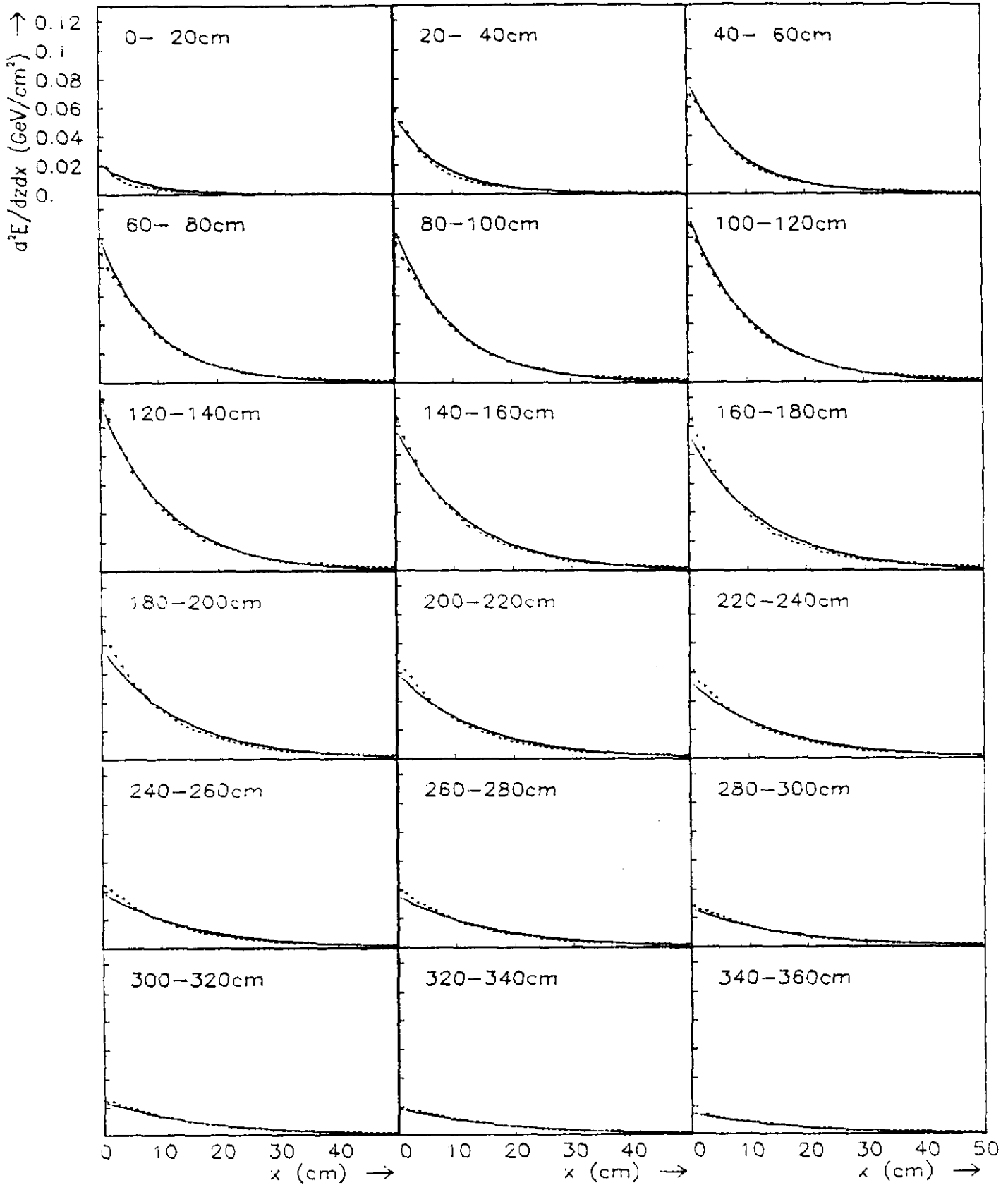


Figure 10(e)

415.4 GeV

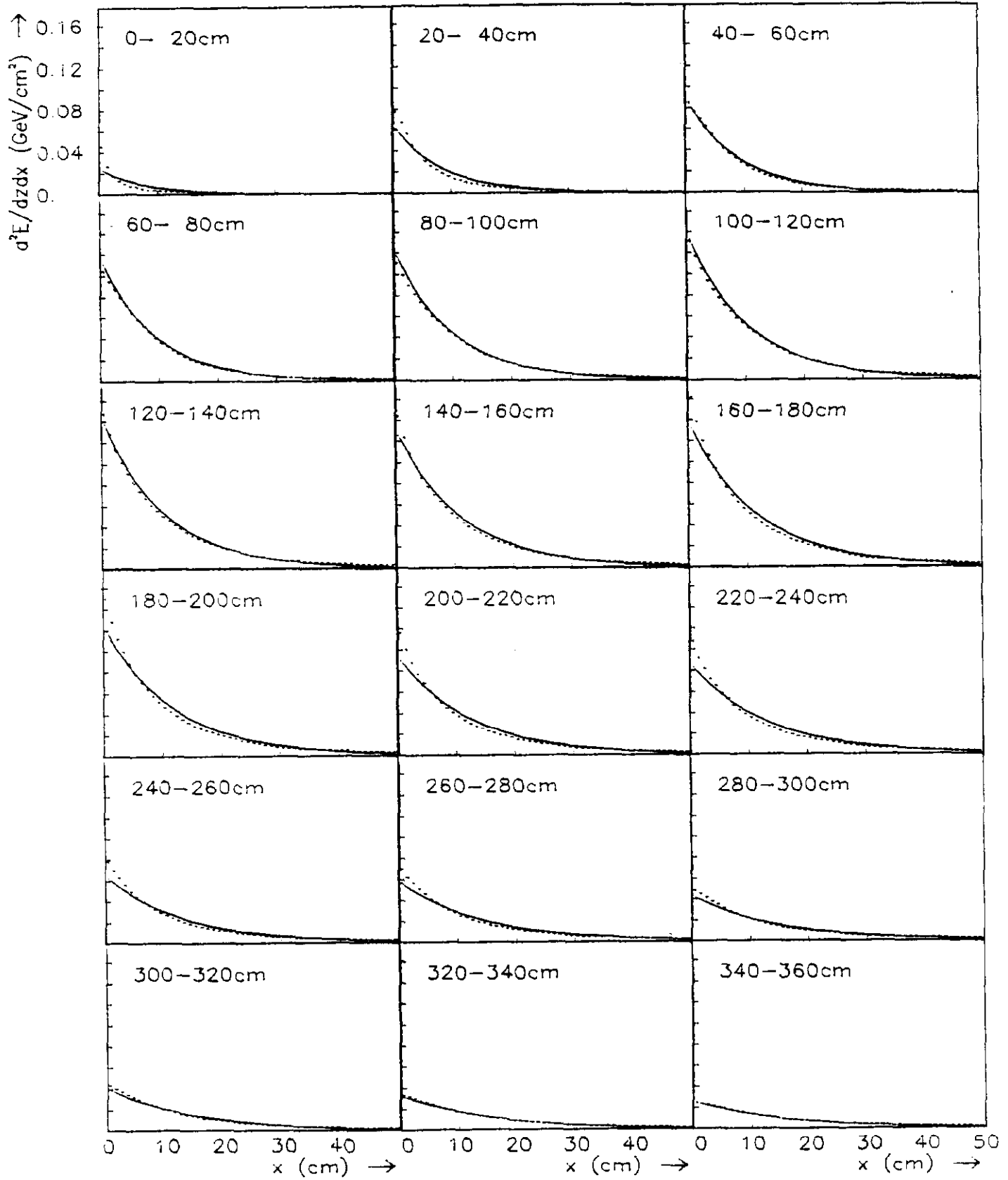


Figure 10(f)

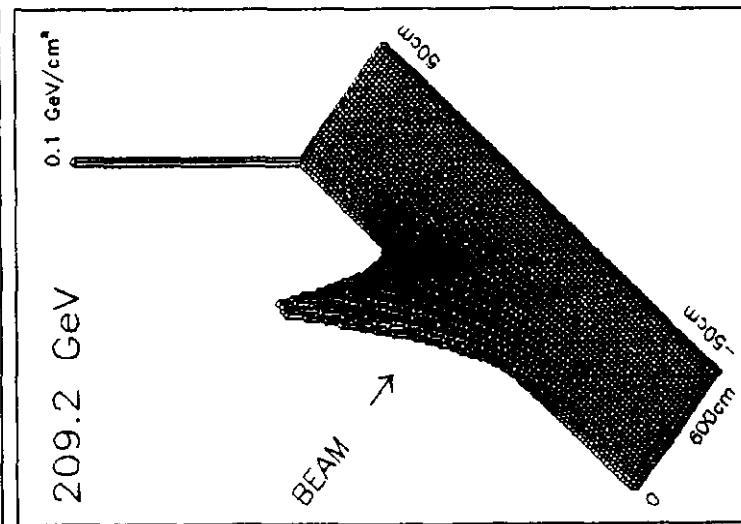
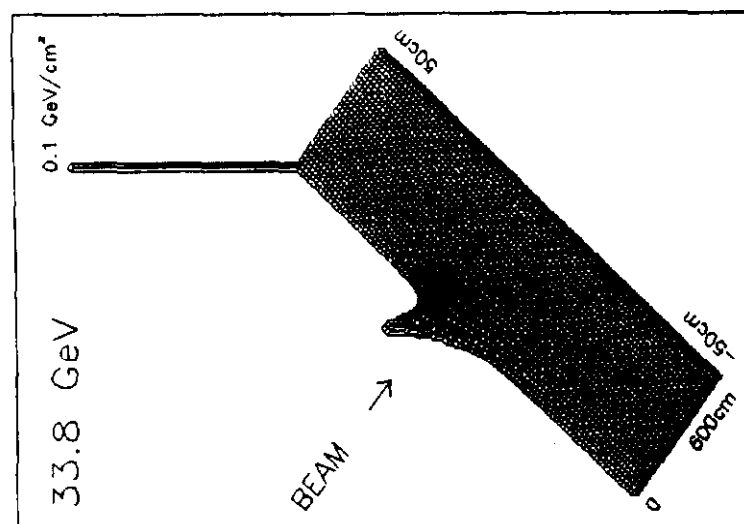
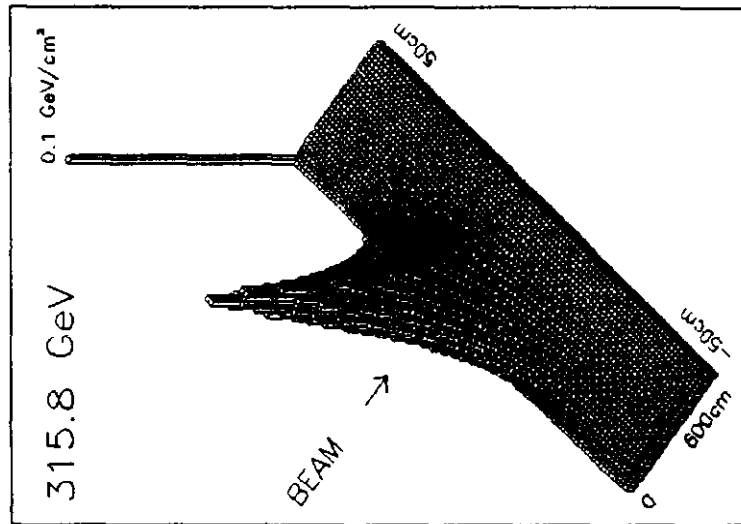
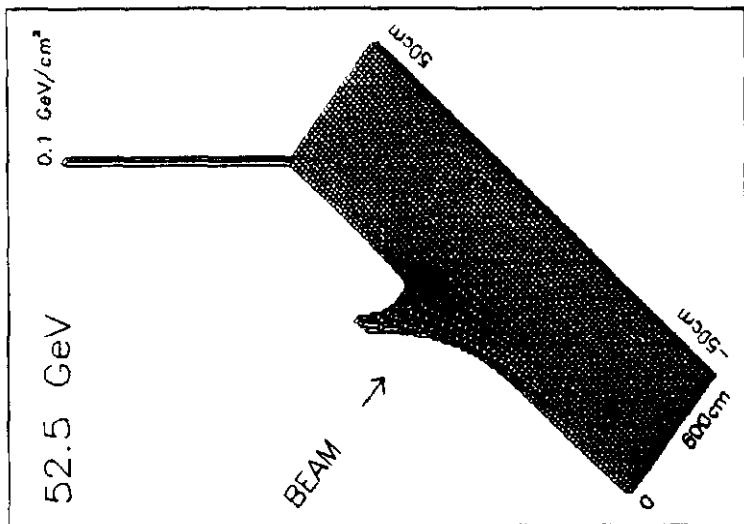
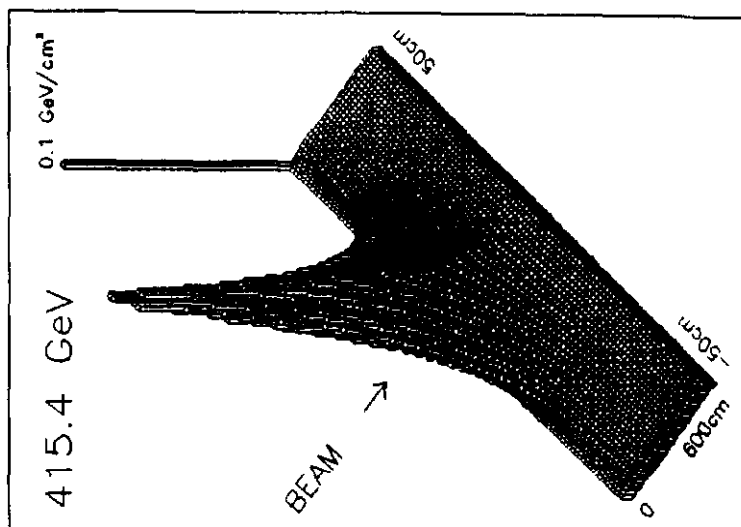
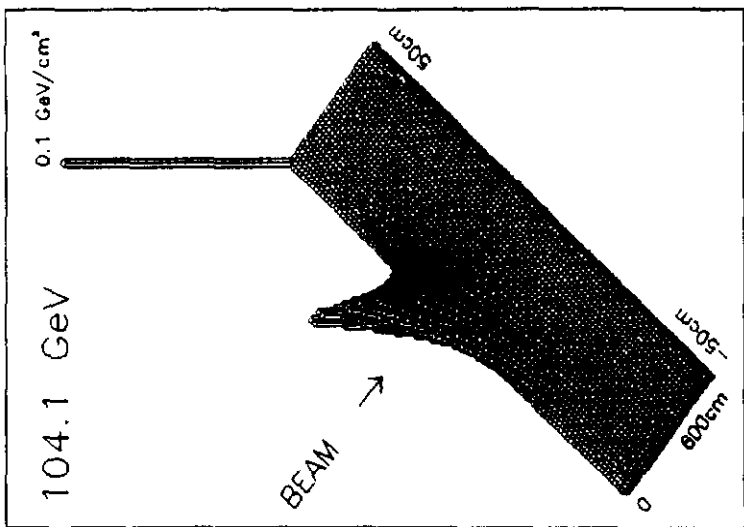


Figure 11

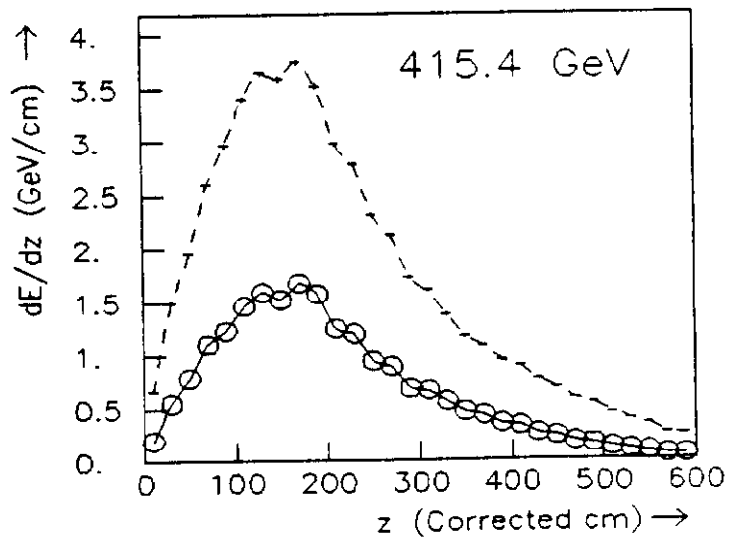
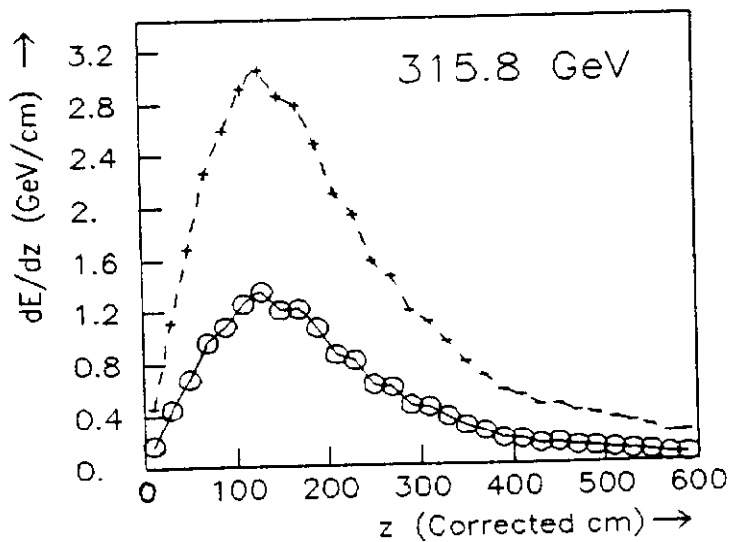
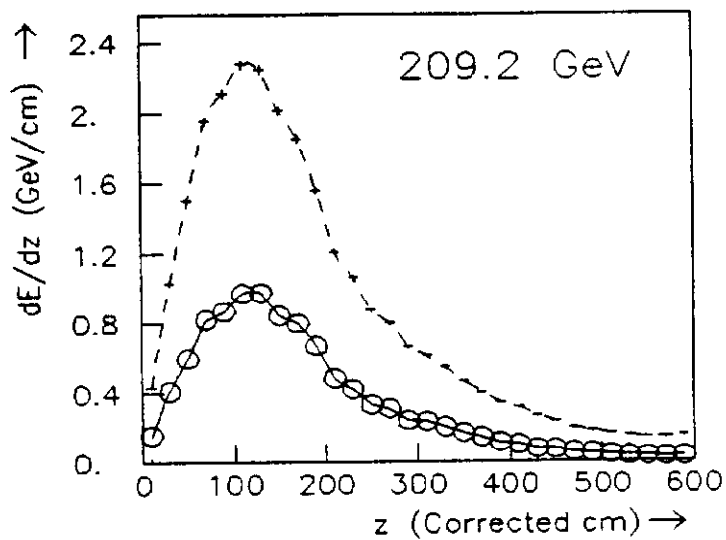
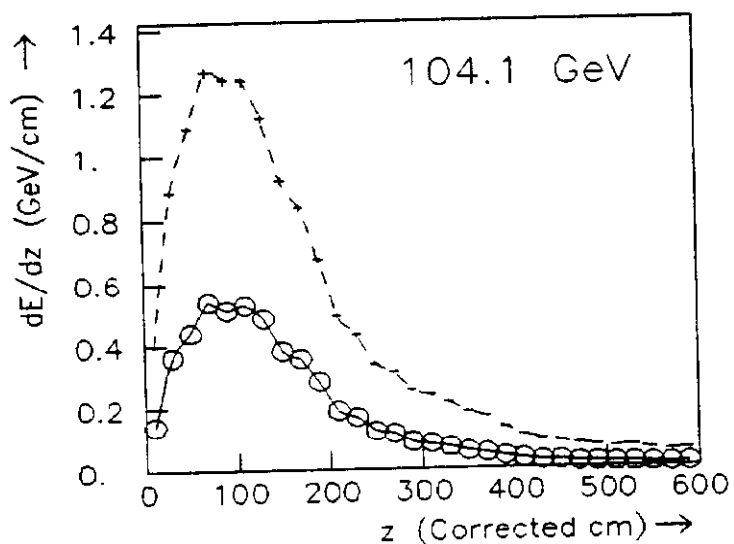
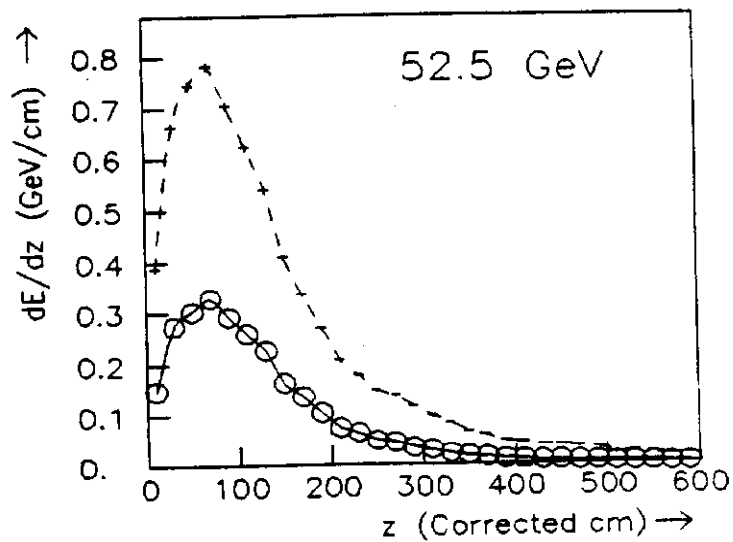
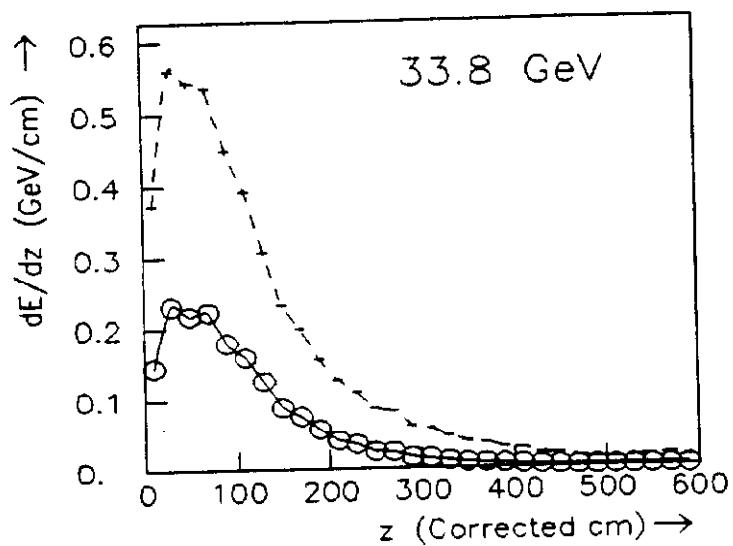


Figure 12

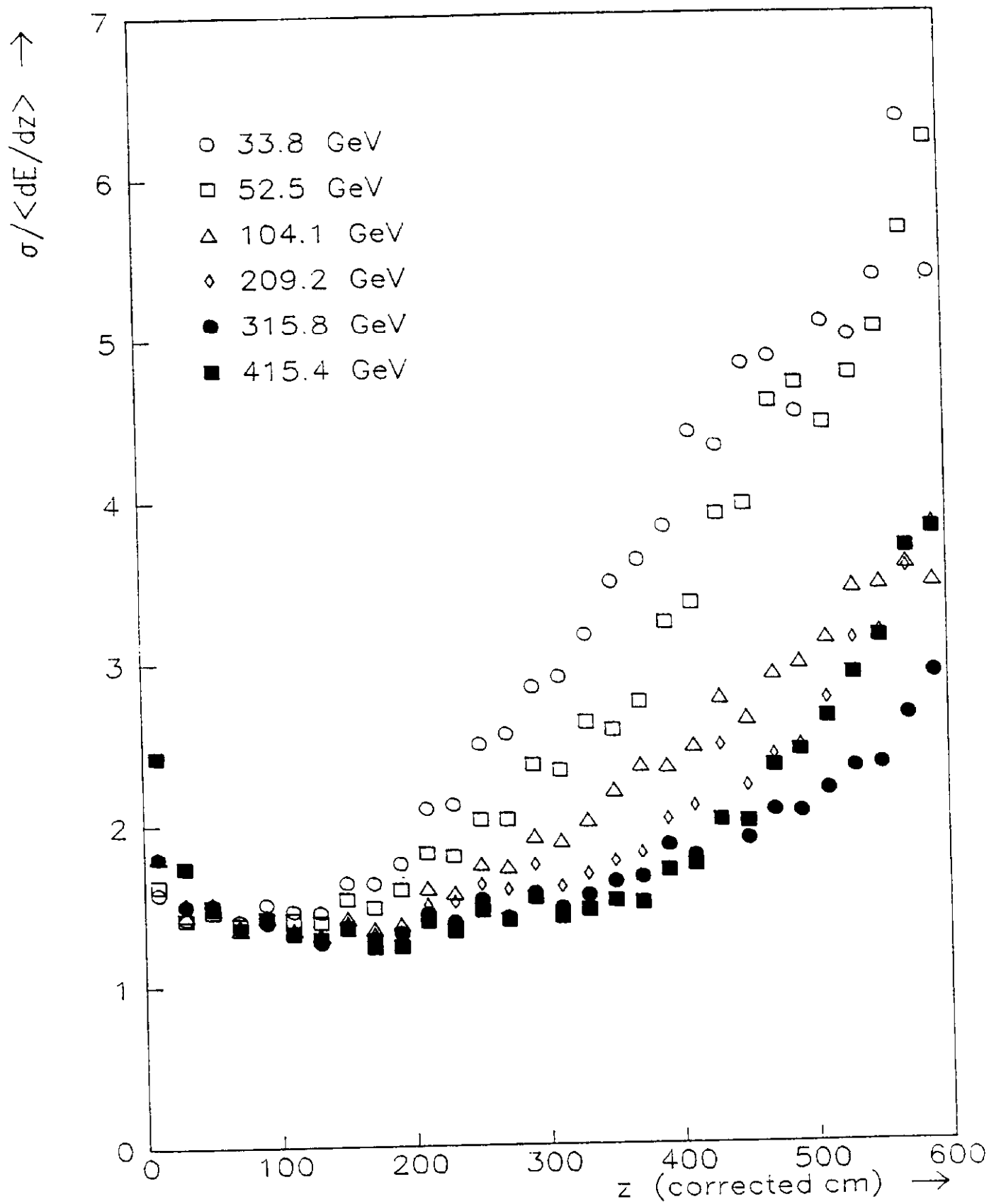


Figure 13

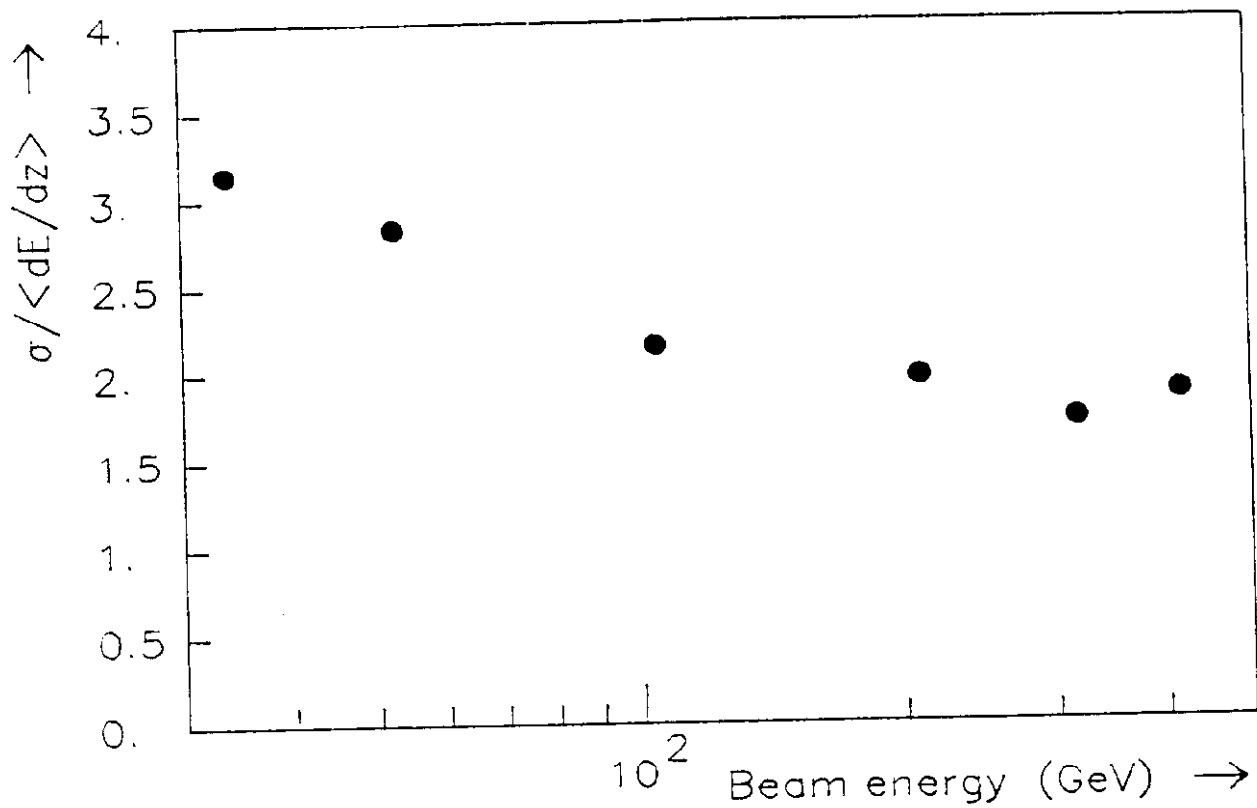


Figure 14

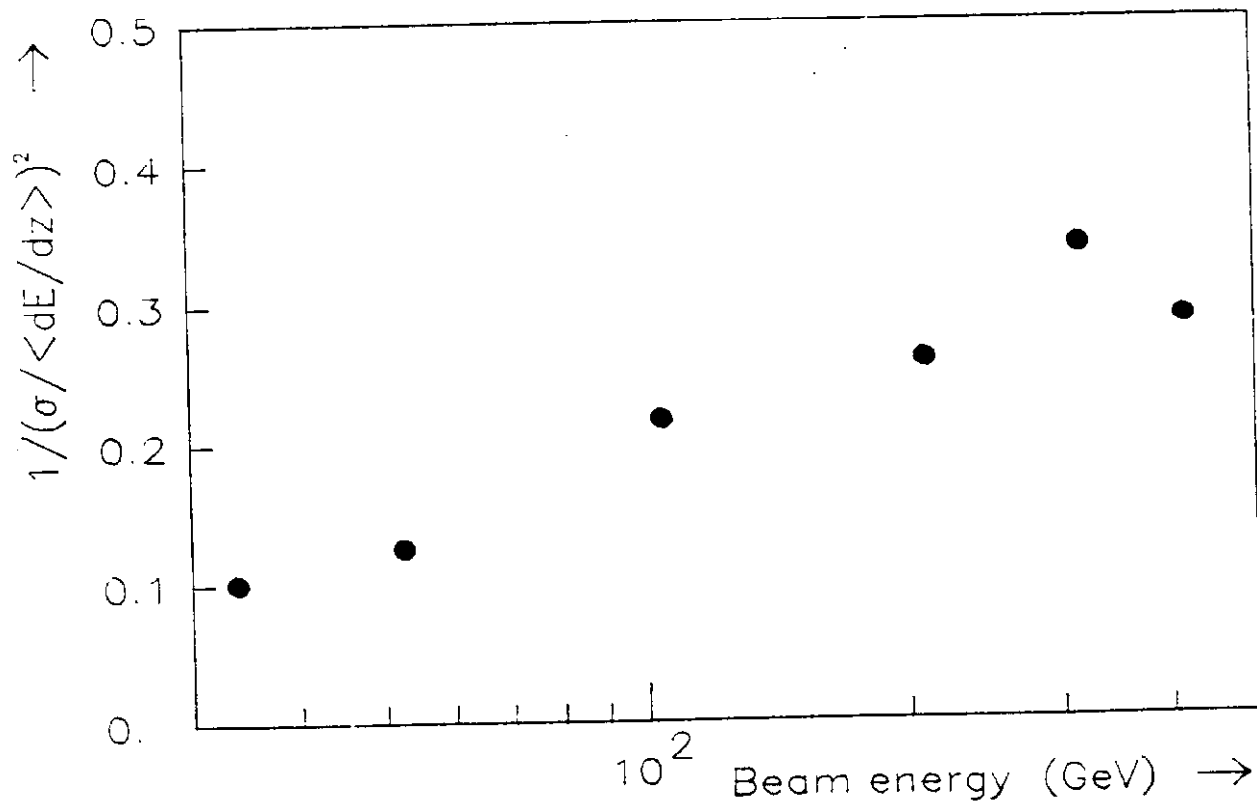


Figure 15

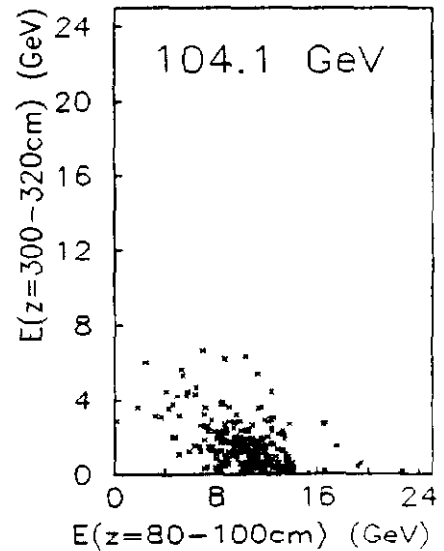
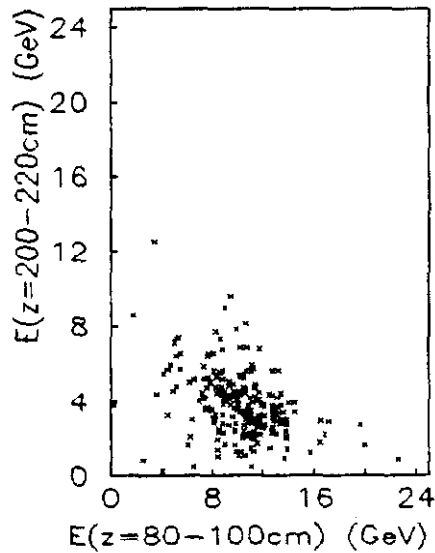
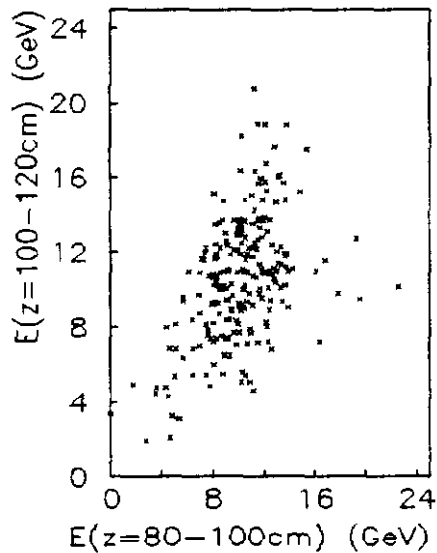
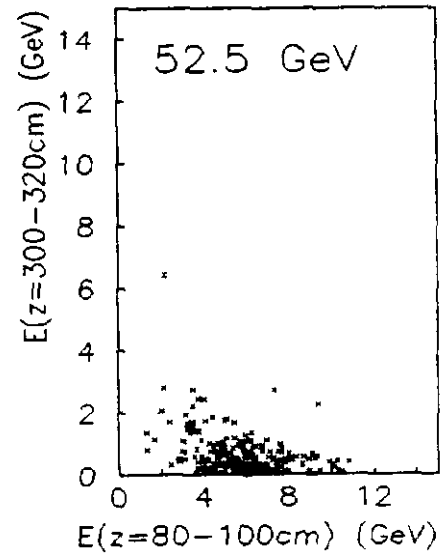
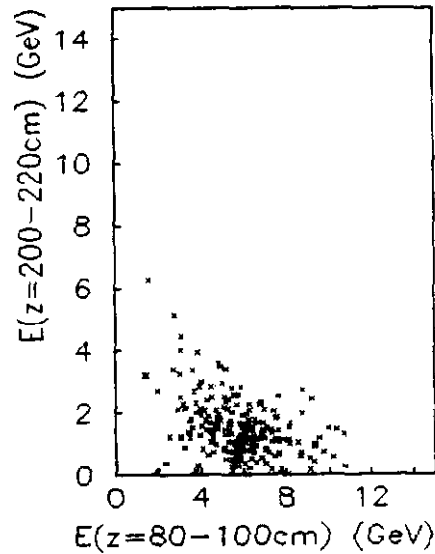
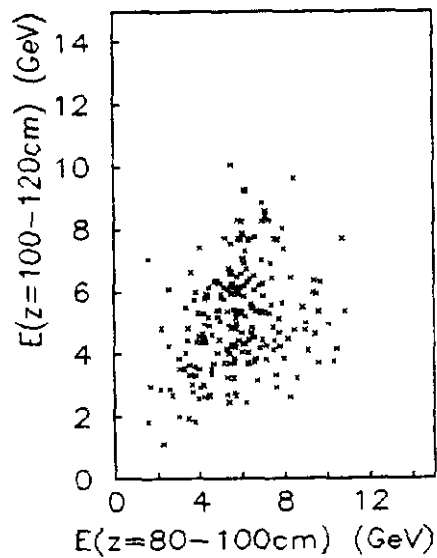
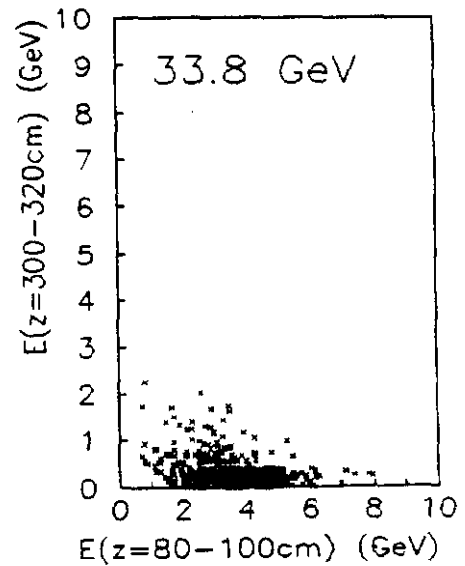
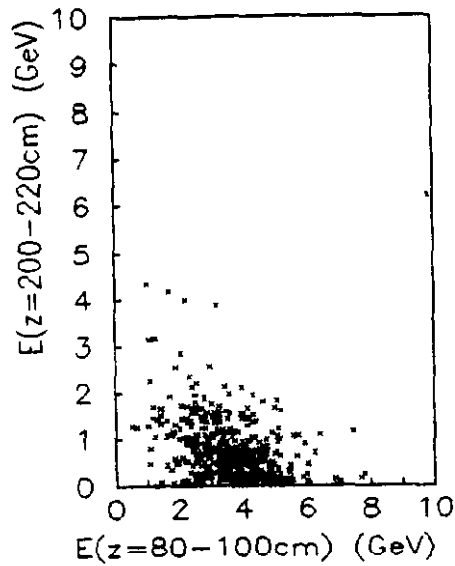
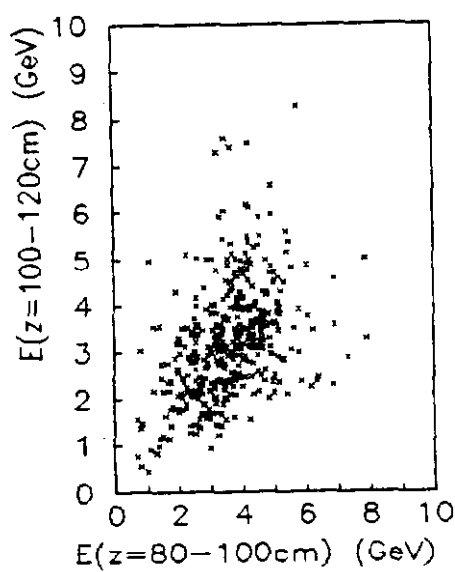


Figure 16

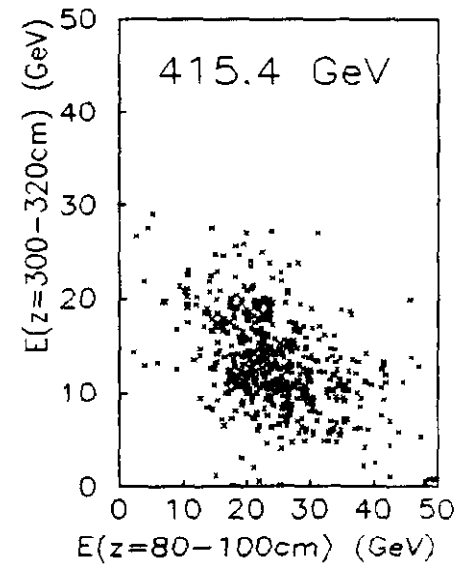
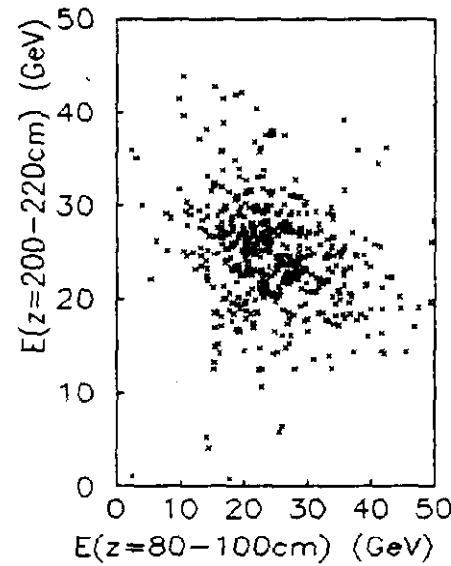
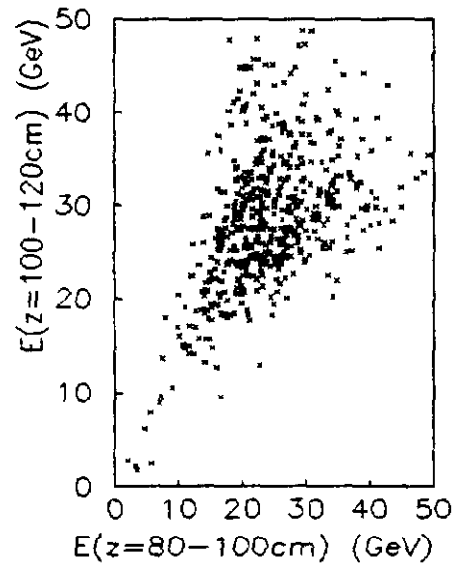
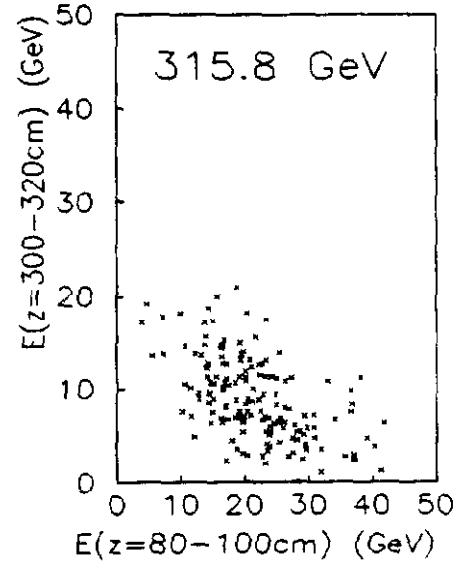
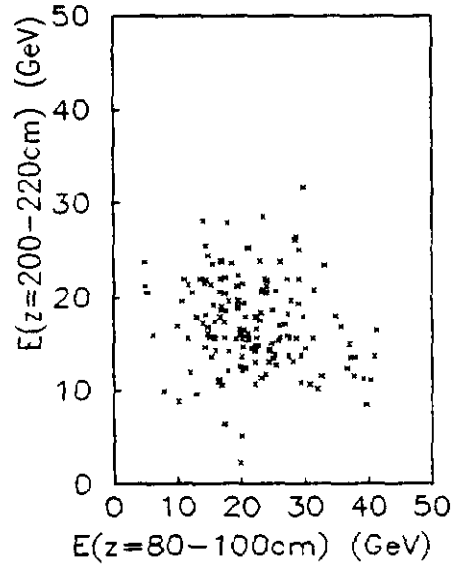
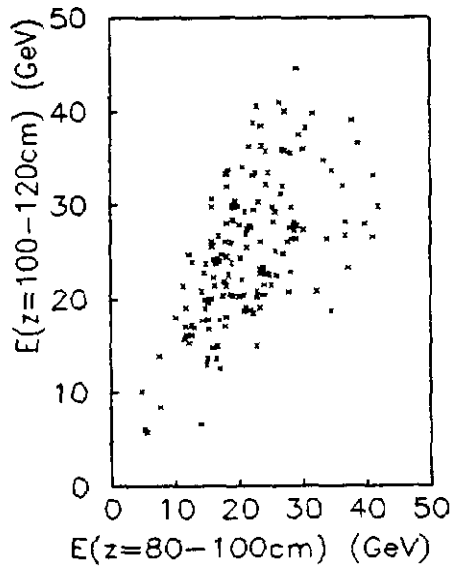
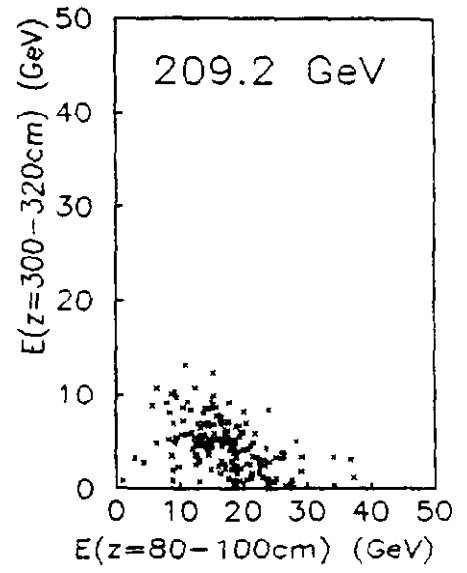
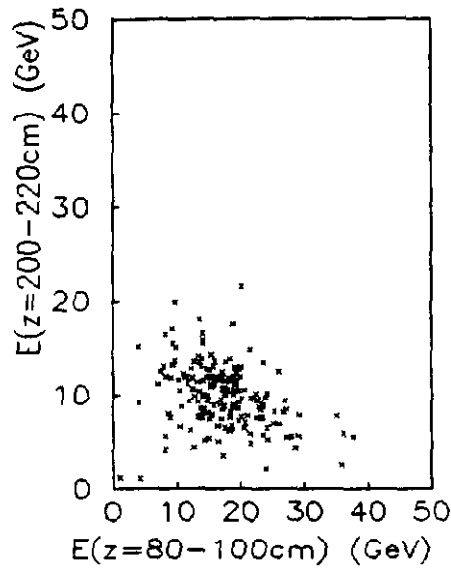
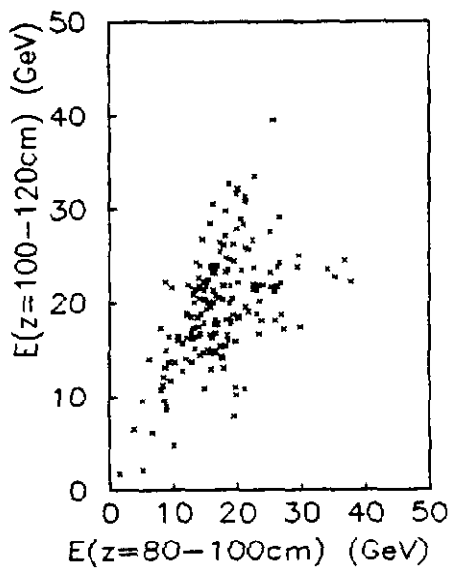


Figure 16 (continued)

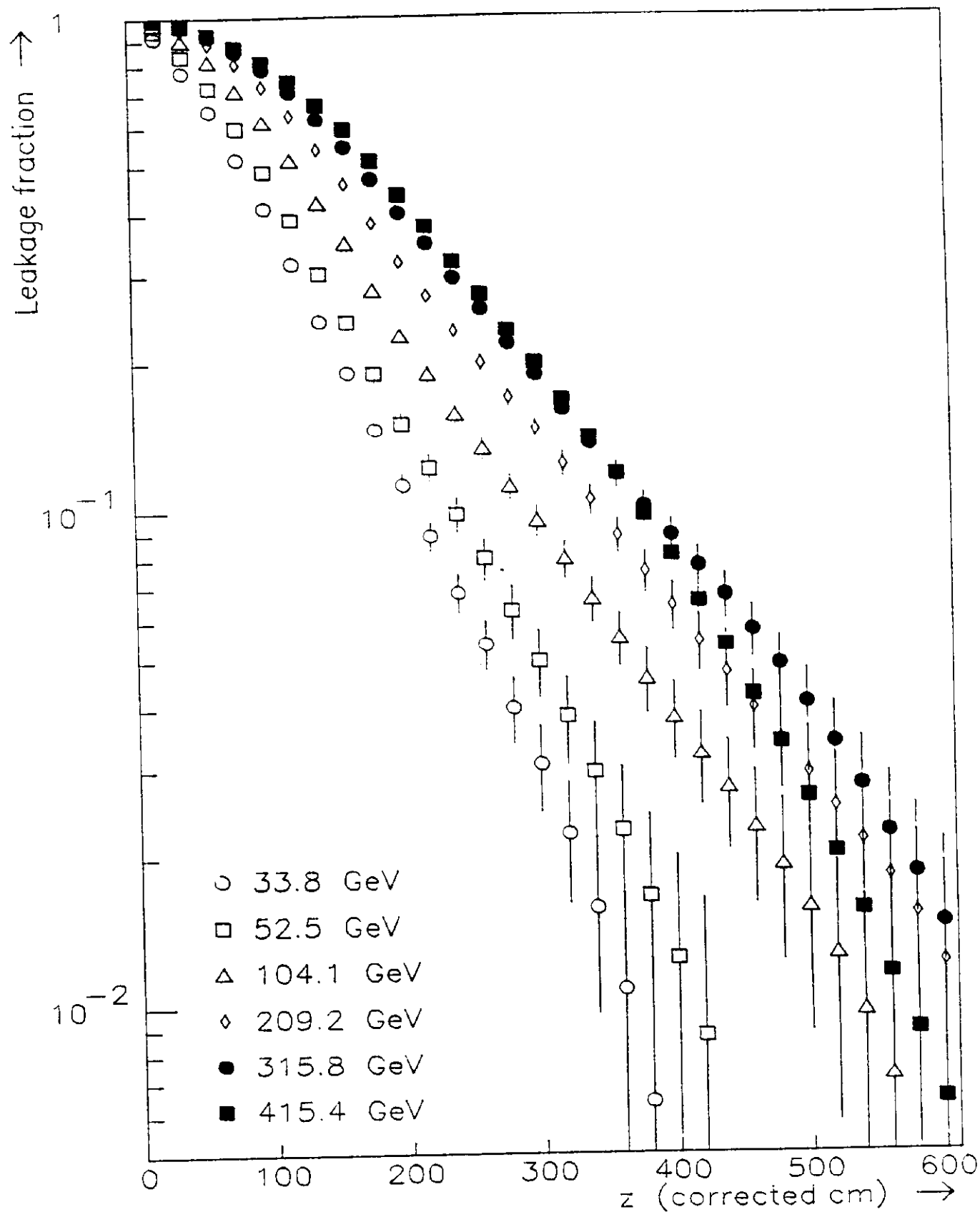


Figure 17

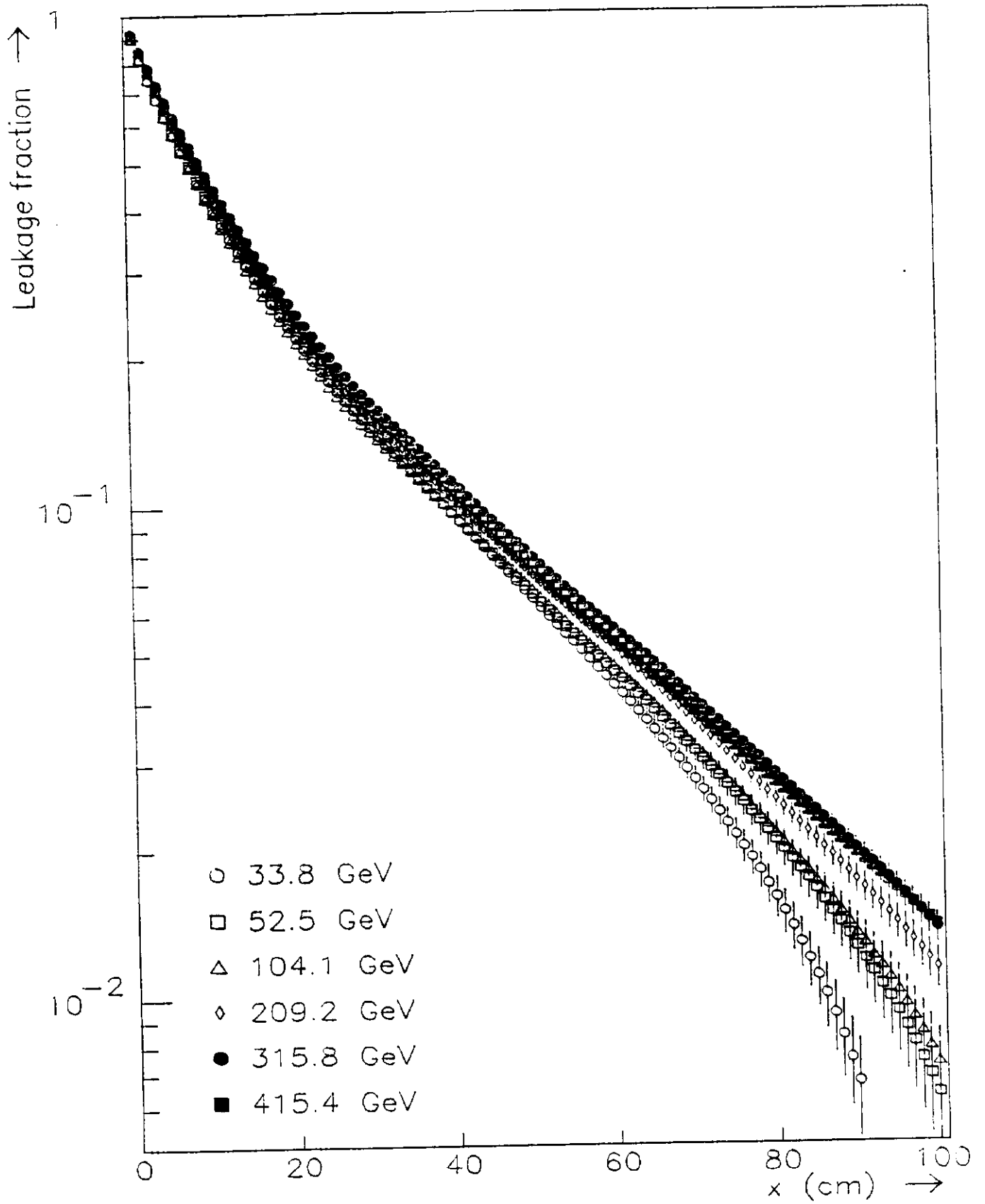


Figure 18

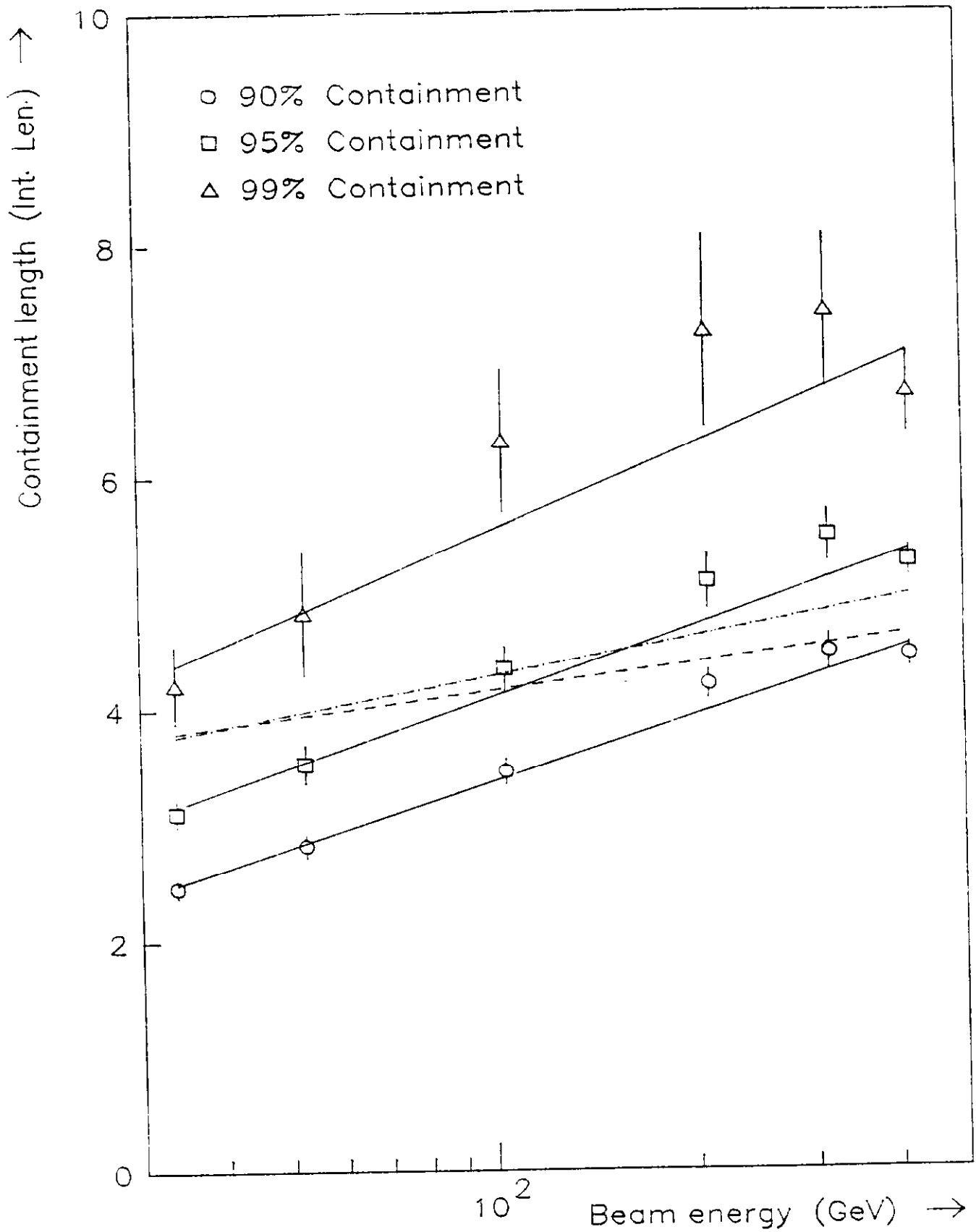


Figure 19

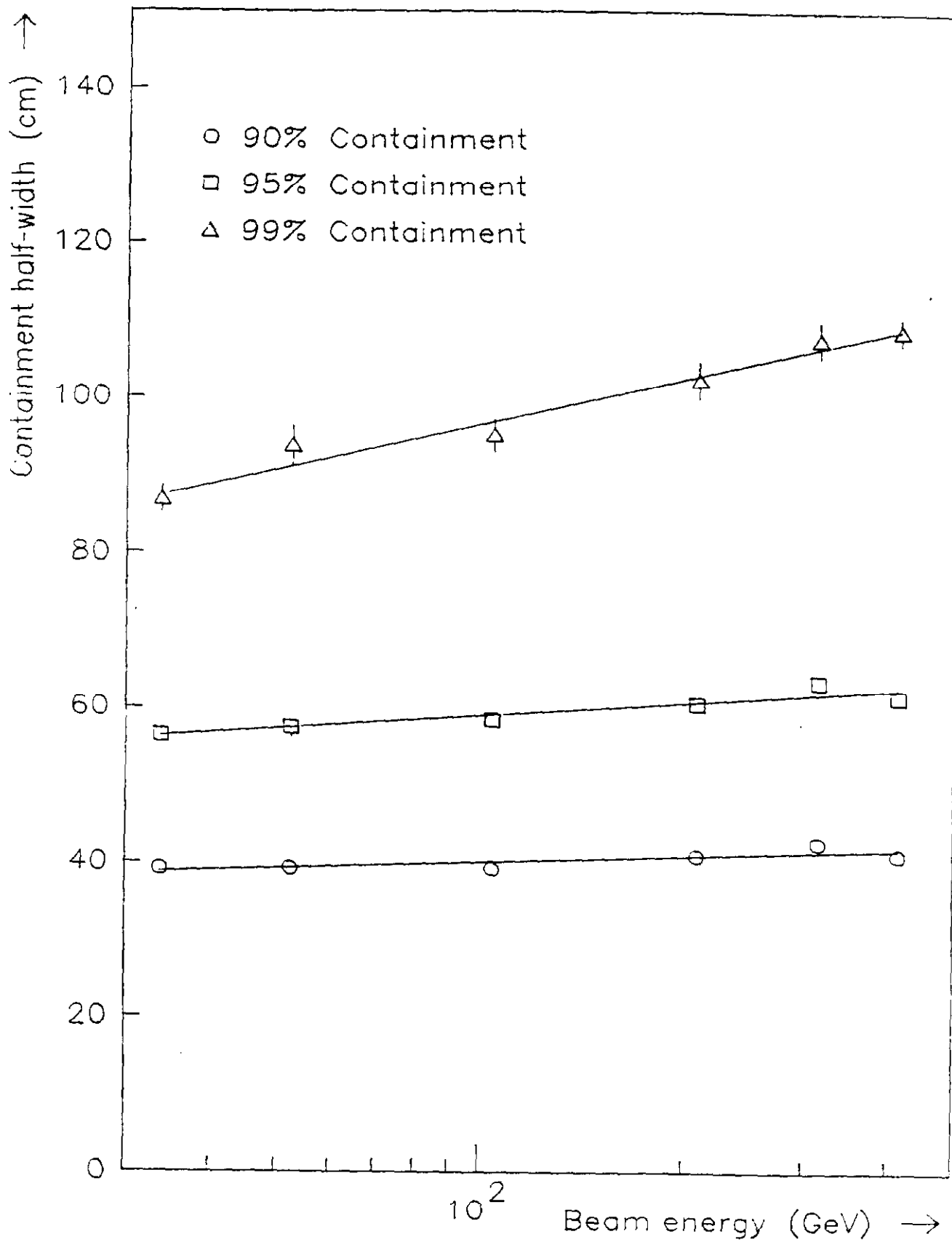


Figure 20